



Porous starch embedded with anthocyanins-CMC coating as bifunctional packaging with seafood freshness monitoring properties

Ana Isabel Quilez-Molina^{a,b,*}, Danila Merino^c, Michel Dumon^a

^a Laboratoire de Chimie des Polymères Organiques, University of Bordeaux, CNRS, Bordeaux INP, LCPO UMR 5629, F-33607 Pessac, France

^b BioEcoUVA Research Institute on Bioeconomy, University of Valladolid (Spain), Calle Dr. Merzelina, 47011, Valladolid, Spain

^c POLYMAT, University of the Basque Country UPV/EHU, Avenida Tolosa 72, Donostia-San Sebastian 20018, Gipuzkoa, Spain

ARTICLE INFO

Keywords:

Food-freshness indicator
Smart food-packaging
Functionalized-starch
Carboxymethyl cellulose
Active coating

ABSTRACT

In line with the growing demand for more sustainable and efficient materials for food packaging, new bifunctional pH-responsive composites were developed with the dual purpose of packaging and indicating seafood spoilage. Within this study, a fully bio-based composite based on porous starch (PS) was prepared via microwave irradiation ($\sim 1 \text{ g/cm}^3$) followed by functionalization via dip-coating with an active solution of anthocyanins-carboxymethyl cellulose (CMC). Here, the edible anthocyanins (Ath) endowed excellent antioxidant and pH-sensing properties to the resulting bifunctional composite (PS-ACMC), covering a pH range of 6–11.5, making it compelling for developing smart food-packaging materials. Moreover, results indicated that the coating scarcely altered the excellent mechanical properties developed by the PS sample, which were comparable with the commercial expanded polystyrene foams. Concurrently, to enhance the competitive properties of the starch component, bifunctional PS-CMC systems were devised crosslinking starch with citric acid. The obtained citrate-starch specimens exhibited a superior porous structure with lower density ($\sim 0.61 \text{ g/cm}^3$), antioxidant properties, and about 40% less solubility in water compared to the neat starch sample. Remarkably, this functionalization hindered the colour-switching properties when the active coating was added, likely due to a strong fixation of the CMC with the natural dye. However, PS-ACMC composites exhibited a rapid and effective colour response, transitioning from violet to greenish-blue, facilitating visual and real-time assessment of the freshness when using shrimp as test specimens. The results reported underscored the high potential of such bifunctional bio-composites in obtaining sustainable and smart freshness-monitoring packaging for seafood.

1. Introduction

The negative environmental impact derived from the production and disposal of petrochemical single-use plastics has promoted the development of new biodegradable materials using sustainable methods. Plastic foams are widely used in packaging due to their cushioning, isolating, and lightness characteristics, which protect and preserve the product while reducing the cost of transport (Nechita & Năstac, 2022). The most used plastic foam is petroleum-derived expanded polystyrene (EPS) due to its versatility, lightweight, rigidity, and foamability features (Uttaravalli et al., 2020). However, polystyrene (PS) has also shown a very low biodegradability and recycling rate, becoming one of the major post-consumer waste products, comprising around 10 wt% of the total plastic waste produced annually in the last ten years (Uttaravalli et al., 2020). Therefore, there is an enormous necessity for

developing biodegradable and sustainable substitutes to reduce the environmental problems caused by this array of synthetic materials used for packaging applications. Some biodegradable alternatives proposed are corrugated board, honeycomb board, and moulded pulp, however, their weak mechanical robustness and poor water resistance strongly limit their practical use (Nechita & Năstac, 2022).

Starch biopolymer is presented as a potential substitute for petroleum-derived foams due to its great tunability, processability, and capability to expand producing lightweight materials (Tapia-Blácido et al., 2022). This polysaccharide is widely found in plants (e.g., rice, corn, maize, and potato) in the form of semicrystalline granules composed of 20–30% linear amylose and 70–80% of highly branched amylopectin (Chen et al., 2019; Quilez-Molina & Merino, 2023). Moreover, starch is highly available, non-toxic, cheap, and amenable to organic compost (Tapia-Blácido et al., 2022). In the foaming process of

* Corresponding author. Laboratoire de Chimie des Polymères Organiques, University of Bordeaux, CNRS, Bordeaux INP, LCPO UMR 5629, F-33607 Pessac, France.
E-mail addresses: ana Isabel.quilez@uva.es (A.I. Quilez-Molina), danila.merino@polymat.eu (D. Merino), michel.dumon@u-bordeaux.fr (M. Dumon).

starch, water acts as a blowing agent and plasticizer, resulting in an easy, safe, and sustainable fabrication methodology (Tapia-Blácido et al., 2022). During heating, water diffuses inside the starch granule provoking granular swelling and starch dissolution (around 70 °C). At higher temperatures, around 180 °C-250 °C, the water transforms into steam, generating pressure inside the matrix and promoting the creation of a cellular structure (Peng et al., 2022; Soykeabkaew et al., 2015; Tapia-Blácido et al., 2022). The processes most used to fabricate starch foams are extrusion and baking, however, starch-based foams can also be assisted by microwave irradiation, which provides a highly effective internal heating reducing the exposure time. This issue can be an advantage for processing thermo-sensitive molecules, as well as to reduce cost and save energy (Brasoveanu & Nemanu, 2014; Golachowski et al., 2020; Quilez-Molina et al., 2024; Tapia-Blácido et al., 2022). Moreover, the effective, fast, and uniform heating of microwave radiation has prone its use in various fields of chemical synthesis, comprising the starch chemical modification (Jyothi et al., 2007; Wu et al., 2020).

Indeed, these chemical modifications have been contemplated as a potential solution to strengthen the water and mechanical resistance of starch porous materials, which are considered as the main limitations of this biopolymer (Golachowski et al., 2020; W. Zhang, Han, & Zhou, 2023). On another side, citric acid (CA) is widely used to functionalize, via esterification and cross-linking, hydroxyl-rich polymers such as polyvinyl alcohol (PVA) (Diop et al., 2023; Ounkaew et al., 2018), chitosan (Diop et al., 2023; Zhang, Han, & Zhou, 2023; Zhang, Han, & Zhou, 2023), and gelatin (Dai et al., 2020; Zhang, Han, & Zhou, 2023), among others. This chemical functionalization, which does not require the presence of catalysts, is aimed at strengthening some functional characteristics of these polymers, such as the poor water resistance or the mechanical properties (Golachowski et al., 2020; Karma et al., 2022; Zhang, Han, & Zhou, 2023). The literature includes several works that use citric acid to improve starch properties with high interest for food packaging applications (e.g., mechanical resistance, and water adsorption capability) (Golachowski et al., 2020; Reddy & Yang, 2010). However, most of them involve starch granules (Hong et al., 2020; Liu et al., 2020; Zhong et al., 2022), films (Chi et al., 2024; Ciaramitaro et al., 2023; Poudel et al., 2023), or aerogels (Camani et al., 2021, 2023), while studies regarding citrate starch foams or porous materials with promising application in the food packaging field are barely found (Hassan et al., 2020; Pornsuksomboon et al., 2016). Moreover, most of the citrate-derived materials with a promising application as food containers are fabricated through baking (Pornsuksomboon et al., 2016), or compression moulding (Hassan et al., 2020), while the functional features of the citrate-starch composites assessed via microwave irradiation are still unexplored.

On the other hand, coatings have been widely used to improve the poor moisture and mechanical resistance of starch (Merino et al., 2021; Merino et al., 2022). To date, starch has also been coated with other sustainable systems, such as chitosan (Merino et al., 2018; Zhao et al., 2022), or beeswax (Reis et al., 2018), obtaining an improvement in water barrier properties. Additionally, a coating can be also employed to provide additional active properties without altering the morphological characteristics of the substrate (e.g. porous structure). Sodium carboxymethyl cellulose (CMC) is an anionic water-soluble, low-cost, and transparent cellulose derivate, widely employed in food packaging as an edible coating for foods (Cai et al., 2022; Panahirad et al., 2021; Tapia-Blácido et al., 2022). Its structure consists of a linear and long chain of glucopyranosyl units with a high molecular weight that provides strength and structural integrity in food coatings (Panahirad et al., 2021). Different from beeswax coating, which has shown problems of adhesion due to the low compatibility with starch (Chaireh et al., 2020; Reis et al., 2018), CMC has been demonstrated to enhance the functional properties of starch (e.g., mechanical and water vapor barrier properties) when they are assembled constituting a matrix (Tavares et al., 2019; Łupina et al., 2022). However, to the best of our knowledge, the

incorporation of active and superficial CMC-coating in starch-porous structures has not been reported. As said above, the design of superficial laminates or coatings presents additional advantages, such as the possibility to add active molecules able to prompt unique and profitable responses (e.g., antioxidant, antimicrobial, or sensing properties), with high interest for developing smart packaging materials. With the purpose of obtaining these beneficial properties, the polyelectrolyte CMC polymer has been widely used as a host of the natural, antioxidant and colour pH-sensitive molecules Anthocyanins (Ath) (Liang et al., 2019; Sadi & Ferfera-Harrar, 2023). The high efficiency of Ath's encapsulation comes from the inherent charge of these ingredients, negative for CMC and positive for Ath, creating strong electrostatic interactions. Among the different types of Ath, the grape peel presents upstanding antioxidant properties compared to anthocyanins derived from other plant sources (Kan et al., 2022).

Based on the overhead background, the present work introduces a new type of fully-biobased and active bifunctional composites as a promising candidate for substituting the polluting above-mentioned packaging plastics. These composites were elaborated by coating a porous starch matrix, prepared via microwave irradiation, with an active Ath-CMC solution. In such a manner, the grape peel-derived Ath molecules successfully endowed antioxidant and pH-coloring sensing responses to the tridimensional starch matrix without affecting its original morphology and excellent mechanical properties. On the other hand, the great encapsulation capability of CMC impeded the release of Ath in a fatty-food simulant, ensuring a stable and durable response of the composite under these conditions. Moreover, the fabricated bifunctional starch-CMC trays displayed a clear and effective colour change in response to the shrimp spoilage during real-time experiments, underscoring the potential application of this material as sustainable and intelligent food packaging. Moreover, profiting from the high versatility and performance of microwave treatment in the functionalizing macromolecules, the same procedure was tested on improved porous starch materials (citrate-starch). This approach, aiming to improve the foamability and certain functional properties of the previous composites, resulted in higher porosity and decreased density, but at the cost of a complete depletion of the pH-responsive properties. To our knowledge, this study examines for the first time the combination of these two components in such a particular design as a novel approach to developing colourimetric pH-sensitive food packaging materials.

2. Experimental section

2.1. Materials

A native rice starch (labelled RS), Carboxymethyl cellulose sodium salt (Mw ~ 90,000), citric acid, and sodium hydroxide were purchased by Sigma Aldrich. The anthocyanin powder obtained from the grape peel was purchased from Jeulin (France). Finally, the shrimps with heads were purchased from a local Spanish grocery store.

2.2. Methodology

2.2.1. Esterification of rice starch

The esterification of the RS was achieved using the method reported by Ma et al. (2009), Liu et al. (2020) with slight modifications. As shown in the scheme of Fig. 1 (a), 40 g of CA was dissolved in 100 mL of water, and the pH of the solution was adjusted to 4 with a 10 M NaOH solution (Liu et al., 2020; Ma et al., 2009). Once conditioned, 100 g of RS was mixed with the solution and stirred at room conditions for 12 h to favour the mixing. Afterwards, an opaque whitish suspension was obtained, which was subsequently poured into a crystallization dish ($\varnothing = 15$) and dried for 6 h at 60 °C followed by 90 min at 130 °C in an oven Memmert UF55plus-Universal (Ma et al., 2009). These heating conditions promoted CA dehydration, forming highly reactive anhydride species, which react with the hydroxyl groups of starch forming an ester and

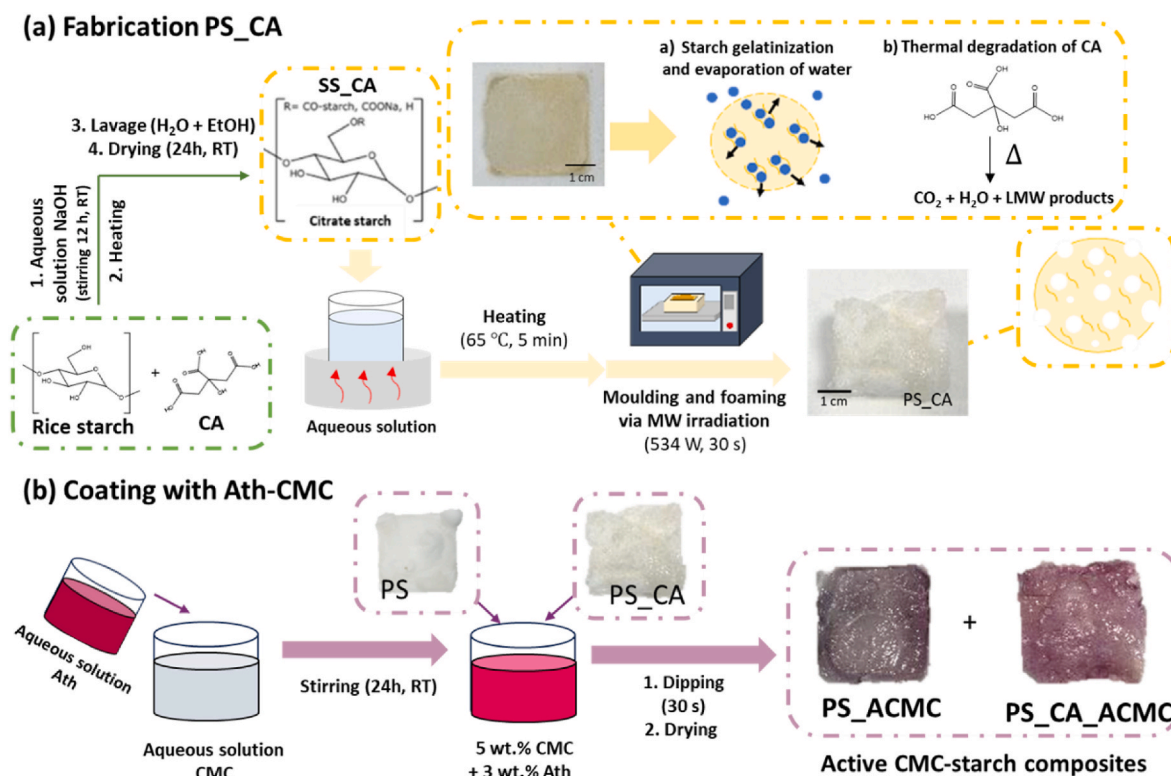


Fig. 1. (a) Fabrication scheme of porous citrate starch samples (PS_CA), where the citration reaction of starch is marked in green, while the expansion process is in yellow. (b) The scheme of the coating process for obtaining the starch composites coated with a layer of CMC-Ath labelled PS_ACMC and PS_CA_ACMC. Labels: CA citric acid, CMC carboxy methyl cellulose, Ath anthocyanins.

incorporating the acid into the starch chains (Ma & Wang, 2016; Sánchez-Rivera et al., 2017). Then, the residual CA was removed by washing the starch with water and ethanol (Liu et al., 2020; Ma et al., 2009). The resulting functionalized starch was dried under a hood for 24 h before the microwave treatment. The resulting product, labelled SS_CA, was a highly rigid and yellowish solid. As (Liu et al., 2020) reported, 40 wt% of CA (based on starch dry weight) was the optimum concentration for obtaining a high degree of esterification of the matrix.

2.2.2. Microwave treatment

The starch composites were obtained employing a free-expansion fabrication method adapted from our previous work (Quilez-Molina et al., 2024) with some modifications.

2.2.2.1. Neat starch samples. The fabrication of non-functionalized porous starch (labelled PS) comprised the manual mixing of 11.5 g of rice starch with 9.8 g of water. Then, the mixture was poured into a mold of polytetrafluoroethylene (PTFE) ($3.4 \times 3.4 \times 1.4 \text{ cm}^3$), and placed in a microwave (30 s, 534 W). After several attempts, this proportion of starch/water and irradiation conditions were demonstrated to provide the best structural characteristics, like good free-standing and mechanical properties, avoiding the obtention of wet or burnt sample, some examples of unsuitable materials are reported in Fig. S1. The obtained specimen of porous starch was carefully removed from the mould and left to dry under a hood at room temperature for 24 h to allow the evaporation of most of the remaining water molecules. Then, samples were kept in polyethylene (PE) zip bags until further analysis.

2.2.2.2. Citric acid-functionalized starch sample. Fig. 1 (a) represents the fabrication steps for obtaining citric acid-functionalized porous starch samples (labelled PS_CA). First, the solid citrated starch (SS-CA) was soaked in 60 mL of water at 65 °C for 5 min to introduce water molecules into the starch matrix, which are necessary to induce the foaming, as

water steam acts as a blowing agent. Moreover, the remaining free CA molecules also contributed to the foaming process by acting as blowing agents, decomposing into CO₂, water, and low-molecular-weight (LMW) products, see Fig. 1 (a) (Sadik et al., 2018). Preliminary experiments showed that the employment of temperatures above the starch gelatinization temperature (78 °C), resulted in the burn of samples using the same microwave irradiation conditions, see Tg in Fig. S2 and the photograph of the burnt sample in Fig. S3 of Supporting information (Bakierska et al., 2014). This response was associated with the hydrolysis of starch in presence of hot water in acids conditions (Karma et al., 2022; Zhang, Han, & Zhou, 2023). The water immersion turned the samples easily moldable, facilitating their placement into a mould ($3.4 \times 3.4 \times 1.4 \text{ cm}^3$) before the microwave irradiation (30 s, 534 W). The obtained citrated-starch foam was carefully removed from the mould and left to dry under a hood at room temperature for 24 h to allow the evaporation of the remaining water molecules. Then, samples were kept in polyethylene (PE) zip bags until further analysis. The characteristics of citrate foams were compared with neat starch foams fabricated under the same irradiation conditions, see in detail hereinafter.

2.2.3. Coating of samples

As shown in Fig. 1 (b), PS and PS_CA were dipped in 20 mL of 5 wt% CMC aqueous solution during 30 s to create a superficial and colorless coating layer. Then, the coated samples labelled as PS_CMC and PS_CA_CMC were removed from the solution and dried under the hood overnight. A second drying cycle was performed by putting the samples in the vacuum oven for 6 h at 40 °C to ensure the complete evaporation of the residual water. Such concentration of CMC was shown to be suitable for developing responsive films based on Ath-CMC mixture with excellent pH-responsive properties (Sadi & Ferfera-Harrar, 2023). Moreover, the great susceptibility of starch to moisture requires highly viscous coatings that can prevent the inward transfer of water and alteration of inner structure. Once fabricated, an exhaustive visual

inspection of the sample cross-section denoted the preservation of the porous morphology of the starch component, thus, evidencing the suitability of the concentration chosen. Active coatings were fabricated by adding 3 wt% of Ath with respect to CMC to the solution in 20 mL of water. The coating process was performed following the dipping and drying methods described previously. The amount of coating was similar for both PS and PS_CA, 0.052 g \pm 0.004 g coating/g sample, with imperceptible differences between CMC and Ath-CMC coatings. To gauge their active properties, we compared these coated starch composites with films produced through the casting of a CMC and Ath solution, designated as ACMC films. Noticeably, the intense colour obtained in the coatings or casted films was comparable with the one obtained in other colour-responsive films containing higher concentrations of Ath, such as the κ -carrageenan film with 6 wt% of extractives from grape skin (Chi et al., 2020). These differences in colouration can be justified by the type of Ath powder used. Most of the works employed the rich-in-anthocyanins powders obtained after treating the grape peel, while here, the commercial anthocyanin powder was used.

2.3. Characterization of starch composites

2.3.1. Differential scanning calorimetry (DSC)

The thermal properties of the developed materials were assayed by differential scanning calorimetry (DSC) using a Mettler DSC30 differential-scanning calorimeter (Mettler-Toledo, Columbus, OH, USA). The specimens were heated from 0 °C to 105 °C at a heating rate of 5 °C/min in a nitrogen atmosphere. The raw mixtures containing neat starch powder with water, and wet CA-starch gel, were measured in triplicate, and the gelatinization temperature (T_{gel}) obtained for each sample was represented in terms of average \pm standard deviation (SD). The DSC of starch was done by heating from -20 °C to 110 °C at a heating rate of 5 °C/min in a nitrogen atmosphere, cooled at the same rate to 20 °C, paused at 20 °C for 5 min, and finally reheated to 110 °C.

2.3.2. Degree of esterification (ED) and degree of substitution (DS)

The values ED and DS were determined following the method employed elsewhere (Ma et al., 2009; Shi et al., 2007) with slight modifications. Approximately 3 g of the citrated sample was placed into a 250 mL conical flask. Then, 50 mL of 75 % ethanol solution was added, and the conical flask was agitated and warmed at 50 °C for 30 min and then cooled to room temperature. Standard 0.35 M aqueous sodium hydroxide solution (20 mL) was added to saponify the ester and let stir for 24 h, reaching a final pH of around 12.8. The excess alkali was back-titrated with a standard 1 M aqueous hydrochloric acid solution. The ED was calculated following Equation (1) reported by Shi et al. (2007):

$$ED = [V_{\text{NaOH}} \cdot N_{\text{NaOH}} - V_{\text{HCl}} \cdot N_{\text{HCl}}] \cdot M_{\text{gluc-CA}} \cdot (100/m) \quad (1)$$

where V_{NaOH} and V_{HCl} are the volumes (L) of NaOH and HCl, respectively. $M_{\text{gluc-CA}}$ is the molecular weight of one glucose ring unit which was substituted by the CA, which corresponds to 174 g/mol, and m (g) is the weight of the citrated sample.

The DS was calculated according to Equation (2) reported by Shi et al. (2007):

$$DS = \frac{(M_{\text{glu}} \cdot \text{mol}_{\text{NaOH}})}{(1 - M_{\text{glu-CA}} \cdot \text{mol}_{\text{NaOH}})} \quad (2)$$

where M_{glu} means the molecular weight of the glucose ring unit (162 g/mol), and mol_{NaOH} is the mole number of NaOH which reacted with 1 g substitute.

2.3.3. Nuclear magnetic resonance (NMR)

Around 20–60 mg of PS and PS_CA, were analyzed in the solid state using Bruker AVANCE II 400 MHz NMR spectrometer. The spectra of CA were obtained by diluting the acid in D₂O (25 mg/mL) and evaluated

with RMN in liquid state with the ¹H NMR and ¹³C NMR using Bruker 400 Ultrashield NMR spectrometer operating at 64 and 128 scans, respectively. The data were processed by Bruker TopSpin 4.09.

2.3.4. Fourier transform infrared (FTIR) spectroscopy

Infrared spectra of the samples were obtained using Attenuated Total Reflectance (ATR) accessory (GladiATR, PIKE Technologies) coupled to a Fourier Transform Infrared (FTIR) spectrometer (Vertex 70, Bruker). All peaks were normalized by the infrared peak at 990 cm⁻¹ for starch sample and 1018 cm⁻¹ for coated samples, which corresponded with the vibration of the skeletal C–O bonds (Camani et al., 2021; Quilez-Molina et al., 2023).

2.3.5. Scanning electron microscopy (SEM)

The morphological study of the samples was performed using a scanning electron microscope HITACHI S-3000 N. For the preparation of the samples, the samples were frozen in liquid nitrogen and fractured to ensure that the microstructure remained intact. Surfaces were coated with gold using a sputter coater (EMSCOPE SC 500) in an argon atmosphere.

2.3.6. Apparent density

The apparent density was calculated by dividing the weight (g) between the volume (cm³) as represented in Equation (3).

$$\rho (\text{g} / \text{cm}^3) = \frac{\text{weight}}{\text{volume}} \quad (3)$$

2.3.7. Thermal gravimetric analysis (TGA)

Thermal gravimetric (TG) curves and the first derivative of the TGA curve (DTG) curve were obtained utilizing a TA Q500 instrument. The samples (~ 20 mg) were heated from 30 to 850 °C under an inert N₂ atmosphere with a flow rate of 60 mL/min and a heating rate of 10 °C/min.

2.3.8. Moisture content, water uptake, and water solubility

The water properties were measured following the procedure published in our previous work with slight modifications (Merino, Bellassi, et al., 2023; Quilez-Molina et al., 2023). The CMC films ($\varnothing = 10$ mm) and starch samples of (3.4 \times 3.4 cm²) were weighed (W_1) and dried in a vacuum oven at 40 °C until reaching a constant weight (W_2). The moisture content was calculated following Equation (4):

$$\text{Moisture (\%)} = \frac{W_1 - W_2}{W_1} \times 100 \quad (4)$$

The experiment was performed in triplicate.

The water absorption capability (water uptake) was calculated following the process reported by (Merino, Mansilla, et al., 2023). Samples (3.4 \times 3.4 cm²) were dried in an oven, weighted (W_{dry}), and placed in 20 mL of distilled water for 24 h. Then, the sample was weighted after removing the excess water using tissue paper (W_{wet}). The water uptake was calculated by difference of weight according to Equation (5):

$$\text{Water uptake (\%)} = \frac{W_{\text{wet}} - W_{\text{dry}}}{W_{\text{dry}}} \times 100 \quad (5)$$

The water-soluble fraction or water solubility was evaluated following the next procedure. First, the samples (3.4 \times 3.4 cm²) were dried in a vacuum oven at 40 °C for 6 h and weighed (W_0). Then, they were immersed in 20 mL of distilled water for 24 h, dried again in a vacuum oven for 6 h at 40 °C, and weighed (W) to measure the water-soluble fraction as indicated in Equation (6).

$$\text{Water soluble fraction (\%)} = \frac{W_0 - W}{W_0} \times 100 \quad (6)$$

All these experiments were performed in triplicate.

2.3.9. Water contact angle

The water contact angle was measured on the selected surface after previous conditioning for 24 h at 23 °C and 50% R.H. The measurement was carried out in a Contact Angle System OCA (Dataphysics) equipment, using a drop of 3 µL of Milli-Q water. The results are an average of five measurements.

2.3.10. Mechanical properties

The mechanical properties were determined by compression tests after conditioning at 23 °C and 50% relative humidity for at least 48 h. The experiment was performed at a constant speed of 2.5 mm min⁻¹ and up to a maximum deformation of 80% on cylindrical samples 2 × 2 cm in diameter and height, respectively. All tests were performed at least five times on a TA HD plus Texture Analyzer equipment (Texture Technologies) equipped with a 30 kg cell size.

2.3.11. Antiradical scavenging activity of migrating substances in hydrophobic food simulant

The radical scavenging activity (RSA) of samples was determined based on the method reported by Yang et al. (2020), with slight modifications. Samples (about 30 mg) were immersed in 2 mL of hydrophobic food simulant (95 % ethanol) for 24 h at room temperature (20 °C). Then, 1 mL of the ethanolic extract was mixed with 1 mL of DPPH radical solution in 95 % ethanol (50 mM). The mixture was maintained in room conditions in darkness for 1 h. The absorbance values were measured at 517 nm using a UV–Vis spectrometer (Agilent Cary 100). The DPPH RSA was calculated following Equation (7):

$$\text{RSA (\%)} = \frac{A_0 - A_{24\text{h}}}{A_0} \cdot 100\% \quad (7)$$

where A_0 is the control, which consists of the mixture of solution 1 mL of the simulant and 1 mL of DPPH, and $A_{24\text{h}}$ is the absorbance of the extraction liquid with the DPPH.

2.3.12. Colour-switching properties with pH

The sensitivity to pH of the coated biocomposites was analyzed as reported in our previous work (Quilez-Molina et al., 2021). Briefly, the ACMC films ($\varnothing = 10$ mm) and ACMC-starch composites (about 3 g) were immersed in a buffer solution of potassium dihydrogen phosphate (KH_2PO_4) and dipotassium phosphate (K_2HPO_4) for pH 6 and 8, or alternatively in buffers prepared with sodium carbonate (Na_2CO_3) and sodium bicarbonate (NaHCO_3) (pH 9 to 11.5). Firstly, the sample was immersed in the buffer solution for 30 s and put under the hood to dry. The colourimetric parameters, such as L, a, b, which represent the lightness, redness-greenness, and yellowness-blueness, respectively, were collected after 24 h (when dried) under the same light and distance by using a free mobile app called “Colour Picker”. These values were used to obtain the total colour difference (ΔE) with respect to the pristine sample, following Equation (8) below:

$$\Delta E = [(L - L^*)^2 + (a - a^*)^2 + (b - b^*)^2]^{0.5} \quad (8)$$

where L^* , a^* , and b^* are the colourimetric parameters of the pristine sample.

2.3.13. Shrimp freshness indicator

For this experiment, trays ($8.3 \times 10 \times 3$ cm³) of ACMC-starch composites were prepared by mixing 64 g of starch with water in the same ratio as described in Section 2.2.2. To provide the desired shape, the starch mixtures were placed in a plastic mould of $8.3 \times 10.5 \times 7.0$ cm³ covered by a second mould of $7.0 \times 10.0 \times 6.5$ cm² to facilitate the expansion in only one direction (thickness). The starch-water mixture was heated for 2 min at 534 W in the microwave, unmolded and dried under the hood for 24 h. Then, the Ath-CMC coating was spread with a spatula on the base of the tray that will be in contact with the storage food and dried under a vacuum oven for 6 h at 40 °C. Before the test,

shrimps with heads were thawed at room temperature (about 20 °C). Afterwards, the shrimps were placed on PS_ACMC trays (about $8.3 \times 10.5 \times 3.0$ cm³) and sealed with transparent PE plastic. As reported in our previous work (Quilez-Molina et al., 2021), the total colour difference (ΔE) calculated using Equation (8) was monitored at different times until obtaining a constant response.

3. Results and discussion

3.1. Characterization of starch samples

As it is widely known, high degrees of ED and SD in modified starch are desired to improve the water and mechanical properties of the composite (Jyothi et al., 2007; Xia et al., 2011). In this study, the PS_CA samples displayed an ED of $32.0 \pm 0.8 \%$ and $0.44 \pm 0.0 \%$ of DS (esterification degree ED and degree of substitution DS). When comparing these results with the literature, the DS values obtained here were slightly higher than the ones reported for citrated starch processed through the vacuum-microwave-infrared assistance method using the same initial amount of CA, which corresponded to 0.3 % (Wu et al., 2020), or superior than corn starch processed through melt blending, which achieved a maximum DS of 0.25 % and ED of 21.6 % (Shi et al., 2007).

Fig. 2 (a) displays the solid-state ¹³C NMR spectra of PS and PS_CA, and the liquid-state ¹³C NMR spectra of CA diluted in a deuterated solution. The peaks for PS showed the typical chemical shifting of rice starch (Katoh et al., 2020; Kim et al., 2017), exhibiting a wide peak at 99–108 ppm corresponding to C-1, a peak at around 85.7 ppm for nonordered structure, a broad peak at 71–82 ppm assigned to C2, C3, C4 and C5, and a peak at 65.3 ppm corresponding to the C6. For the solid-state ¹³C NMR spectra of the PS_CA, the new peaks distinguished at 179.3 ppm and 48.3 ppm proved the esterification reaction between the starch and CA (Kim et al., 2017). The broad peak at 179.3 ppm included the ester bond (C7) and non-esterified carboxylic group of CA (C8), while the peak at 48.3 ppm was assigned to the methylene group (C9) (Kim et al., 2017). The assignation of these peaks can be confirmed by inspecting the peaks present in the liquid-state ¹³C NMR of the CA, found at 176.7 ppm, 173.3 ppm, 73.2 ppm, and 43.2 ppm. The peaks in the range of 170 ppm corresponded to the carbonyl groups of the carboxylic group, 176.7 ppm for C8 and 173.3 ppm for C11, while C10 and C9 were assigned to the peaks located at 73.2 ppm and 43.2 ppm, respectively (Kim et al., 2017). The lack of signal at 173.3 ppm in the spectra of PS_CA claimed the absence of free molecules of CA in the sample.

Furthermore, the starch functionalization was also analyzed through infrared spectroscopy, reported in Fig. 2 (b, c). The infrared spectra of the PS sample displayed the typical peaks of starch biopolymer, including the broadband at 3600–3000 cm⁻¹ associated with the stretching of O–H bonds, the vibration peak of C–H bonds at 2925 cm⁻¹, the stretching of the C–O–C groups at 990 cm⁻¹, while the peak at 1640 cm⁻¹ was assigned to the water molecules bonded to the starch (Camani et al., 2021; Quilez-Molina et al., 2023). Parallely, the effect of the microwave treatment on the starch modification was evaluated by analyzing the infrared spectra of the SS_CA (esterified starch before microwave irradiation), represented in the same Fig. 2 (b). The new peak appeared at 1717 cm⁻¹, which was correlated to the stretching vibration of the ester bond, ν (CJO), evidenced that the esterification reaction occurred before the microwave treatment. The success of this reaction was also verified by noticing that the peak of the ester group (1722 cm⁻¹) did not overlap with the CJO stretching modes of the carboxylic acids of the neat CA powder (located at 1693 cm⁻¹ and 1742 cm⁻¹), see Fig. 2 (c) (Ounkaew et al., 2018; Ramirez et al., 2017). In addition to the ester peak in the SS_CA spectra, a new peak appeared at 1577 cm⁻¹ revealed the presence of sodium citrate carboxyl group (i.e., $-\text{COO}^- \text{Na}^+$) in the sample (Camani et al., 2021). These peaks, also present in the PS_CA, evidenced that a minor proportion of the carboxylic groups of the citrate starch were in form of carboxylate

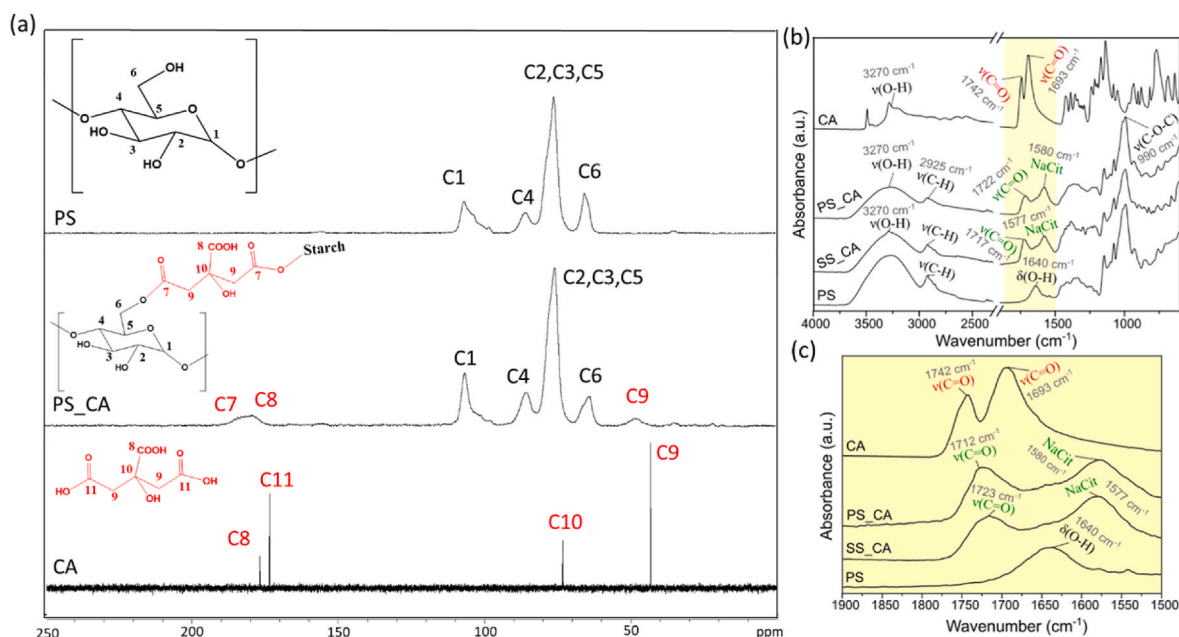


Fig. 2. Assessment of starch functionalization with CA. ¹³C NMR of (a) PS, PS_CA, and CA. (b) The infrared spectra of CA, PS_CA, SS_CA, and PS (c) the zoom-in region (1900–1500 cm⁻¹) of CA, PS_CA, SS_CA, and PS.

(-COO⁻), in concordance of the results obtained from the solid-state ¹³C NMR spectra (Fig. 2 (a)) (Camani et al., 2021; Cuba-Chiem et al., 2008). It's worth mentioning that the formation of di-esters with citric acid is very common in citrate starch (Karma et al., 2022). Interestingly, the lower ratio C=O_{ester}/COO_{citrate} in PS_CA with respect to SS_CA suggested that microwave irradiation promoted the formation of ester bonds, as reported by Hu et al. (2021). Finally, the spectra of PS_CA (after microwave irradiation) displayed less intense and broader O-H peak, centered at 3280 cm⁻¹, in comparison with SS_CA. This insight was attributed to the loss of hydroxyl groups due to the esterification and a new rearrangement of the hydrogen bonds (Liu et al., 2020; Quilez-Molina et al., 2020; Yong & Liu, 2020).

3.2. Chemical characterization of CMC-Ath-coated composites

The infrared spectra of CMC film, uncoated porous starch samples (PS and PS_CA), and starch coated with CMC (PS_CMC and PS_CA_CMC) are represented in Fig. 3 (a). Note that the addition of PS and PS_CA spectra, just described above, is given for a comparative purpose. The CMC showed a broad and strong peak at 3270 cm⁻¹ for the vibration of hydroxyl groups, the peak at 2925 cm⁻¹ was assigned to the stretching

vibration of the methylene groups, at 1585 cm⁻¹ and 1410 cm⁻¹ were located the asymmetric and symmetric vibration of the carboxylate group, respectively, and the peak at 1020 cm⁻¹ was assigned to the skeletal C-O-C vibrations of the glycosidic bonds (Sadi & Ferfera-Harrar, 2023). All these bands appeared in the infrared spectra of PS_CMC with remarkable differences. The most significant was the broadening of the carboxylate bands that evidenced the presence of extra-associated interactions, likely between starch and CMC (Anugrah et al., 2023; Liang et al., 2018; Sadi & Ferfera-Harrar, 2023). Contrarily, the hydrogen-bond band appeared less intense in PS_CA_CMC, suggesting that the intermolecular interaction through hydrogen bonds between the CMC and the starch matrix observed in PS_CMC was reduced as a consequence of the lower amount of OH in the citrate starch after the cross-linking reaction, as argued in the infrared section. Finally, the infrared spectra of PS_CA_CMC exhibited the stretching vibration of the carbonyl group corresponding to the ester (at 1717 cm⁻¹) and sodium carboxylate (1580 cm⁻¹), while the characteristic peaks of starch were barely visible in PS_CMC.

In Fig. 3 (b), the chemical interactions between the CMC polymer with the Ath were evaluated by inspecting the infrared spectra of the ingredients, separately, or together as a film (ACMC). The spectrum of the

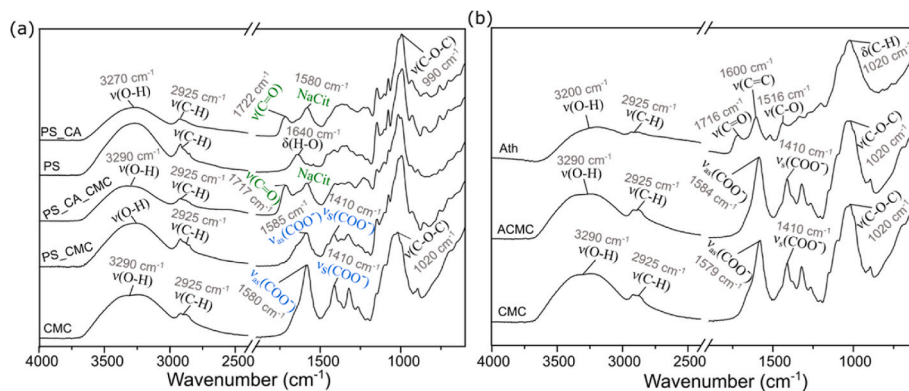


Fig. 3. (a) The infrared spectra of PS_CA, PS, PS_CA_CMC, PS_CMC, and CMC. (b) The infrared spectra of CMC, ACMC, and Ath. The photographs of the films are placed in the inset.

Ath is composed of the vibration of OH groups at 3200 cm^{-1} , the weak band of vibration of methylene at 2925 cm^{-1} , the band at 1716 cm^{-1} corresponding to the carbonyl group, the peaks at 1600 cm^{-1} attributed to the aromatic structure of Ath, and the peak 1020 cm^{-1} which was assigned to the aromatic ring deformation, $\delta(\text{C-H})$ (Ge et al., 2018). The carbonyl group (1716 cm^{-1}) revealed that the Ath was predominately present in the quinoidal base form in the solution (Sadi & Ferfera-Harrar, 2023). The absence of characteristic peaks of the Ath in the APMC film (described above) was related to the low concentration of this additive (3 wt% with respect to CMC). However, the strong colouration of the APMC film confirmed the encapsulation of the natural dye.

3.3. Appearance of samples and colour analysis

Fig. 4 (a) displays the photographs of the surface and the cross-section for the uncoated starch (PS and PS_CA), and starch coated with the CMC-Ath blend, (PS_APMC, and PS_CA_APMC). The uncoated samples displayed remarkable physical differences, indicating that citration induced important physicochemical changes in the starch matrix. PS_CA had a more heterogeneous foamed shape, while PS was smoother and flatter. These features were confirmed by noticing a clear porous structure in the cross-section photographs. This insight was expected as CA acted also as a blowing agent during the microwave irradiation, enhancing the sample foamability (Sadik et al., 2018).

Remarkably, the bifunctional starch-CMC composites displayed the same physical characteristics of the uncoated samples, independent to the presence of Ath, see photographs of Figs. S4 and 4 (a). The high homogeneity and adhesion of the coating highlighted the good compatibility between the two polymers, in agreement with FTIR results. Starch composites acquired a strong colouration after the embedding with the active Ath-CMC mixture, PS_APMC appeared violet, while PS_CA_APMC was pink. Moreover, these samples exhibited some superficial defects (i.e., bubbles or holes) formed during the drying process due to the high viscosity of CMC. However, as will be demonstrated in the following sections, these imperfections did not restrain the performance in the response of the composite. The colour attributes of the uncoated and Ath-CMC-coated samples are collected in Table 1. Herein, the coated PS sample (PS_APMC) displayed slightly more negative values of “b”, indicating a higher blueness, while “a” (redness) was positive in PS_CA_APMC samples corresponding to a pink colour (Alsahag et al., 2023). These remarkable colour differences are related to the protonation/deprotonation molecular switching of Ath and degrees of electron delocalizations (Alsahag et al., 2023). Generally, the positive flavylium cations (AH^+) are red, the neutral base presents a purplish colour (A), while anions are green (A^-) (Alsahag et al., 2023; Yong & Liu, 2020). Under this basis, the violet colour of the PS_APMC was correlated with a superior content of the neutral base (A), which is more stable at slightly basic pHs, as a result of the basic salt sodium carboxylate (CMC), which tends to slightly increase the pH of water.

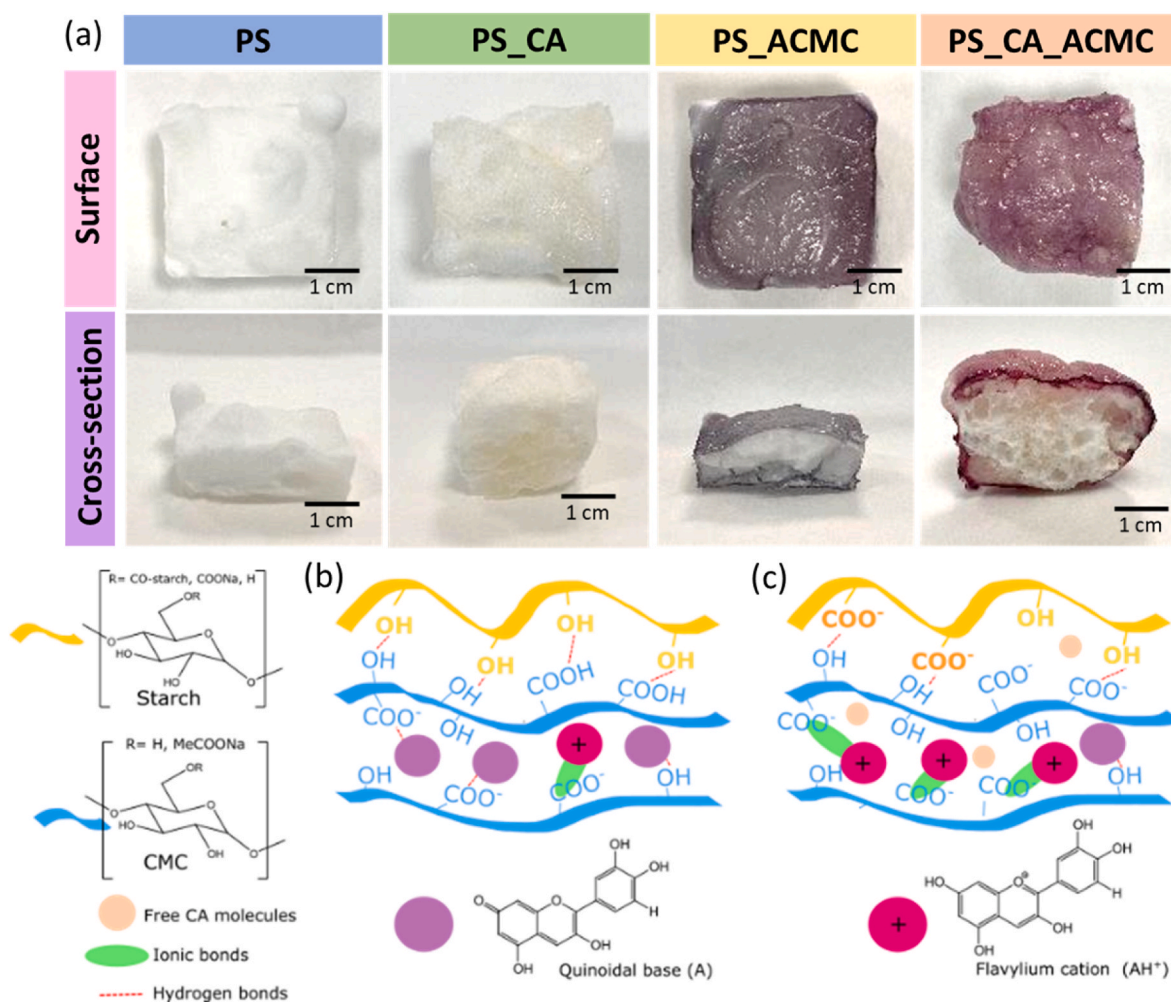


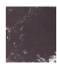




Fig. 4. (a) Photographs of the surface and cross-section of the samples developed in this work. Scheme of the chemical interaction between the CMC and anthocyanins that explain the differences in the colour for (b) PS_APMC and (c) PS_CA_APMC composites. It is recalled that starch foams with a layer of CMC-Ath are labelled PS_APMC and PS_CA_APMC.

Table 1
Photographs and colour parameters of the samples (L, a, and b).

Sample	Colour	L*	a*	b*
PS		71.67 ± 1.55	-1.63 ± 0.00	2.67 ± 0.65
PS_CA		71.13 ± 0.79	-1.95 ± 0.3	8.32 ± 0.20
PS_ACMC		25.75 ± 1.13	3.43 ± 0.5	-2.87 ± 0.91
PS_CA_ACMC		25.31 ± 0.72	15.43 ± 1.62	-1.48 ± 1.11
ACMC		38.17 ± 4.48	6.99 ± 0.43	-11.60 ± 0.12

Regarding the pinkish PS_CA_ACMC sample, the red flavylum cations (AH^+) were the prevalent species of Ath, characteristic of acidic environments. This insight could be justified by the occurrence of a minor amount of free citric acid molecules (not observable through ^{13}C RMN or FTIR) or, more likely, due to partial hydrolysis occurring in the dipping process with the aqueous solution of CMC, resulting in a substantial decrement of the pH. The positive-charged flavylum cations (AH^+) favoured the formation of strong ionic bonds with the carboxylate groups of CMC ($-COO^-$). At the same time, the neutral base (A) was linked through hydrogen bonds, see Fig. 4 (c). Consequently, the responsive properties of these materials will vary considerably.

3.4. Foaming properties: morphology and density of samples

In the microscopical images represented in Fig. 5 (a–b), PS displayed a denser structure with ubiquitous and homogeneous small pores, while PS_CA presented bigger and more irregular pores throughout the structure. As said before, CA acted also as a blowing agent, decomposing thermally into the gases CO_2 and H_2O in the range of 160–270 °C, inducing the formation of pores and the subsequent material expansion

(Sadi et al., 2018). According to the pores size distribution diagram of Fig. 5 (c), PS had a greater number of small cells and a narrower pore size distribution ($0.05 \text{ mm} \pm 0.02 \text{ mm}$) with respect to PS_CA ($0.14 \text{ mm} \pm 0.1 \text{ mm}$). The cell size obtained was in line with the one found in other starch-based composite foams processed through microwave irradiation (Lopez-Gil et al., 2015; Quilez-Molina et al., 2024). The wider pores were assigned to the thermal degradation of the free molecules of CA described above. However, the overall increment of the pore size in the citrated sample can also be explained by an increment of the bubble coalescence due to the higher mobility of the starch chains as a result of the disruption of hydrogen bonds between the starch chains due to the plasticizing effect of CA (Dai et al., 2020). This last insight could also explain the superior expandability properties of the citrate starch.

The cross-section images of the coated samples (PS_ACMC and PS_CA_ACMC) reported in Fig. 5 (d, e) indicated a coating thickness of around 0.25 mm, in both cases. The lack of voids or cavitation between the two polymeric phases underlined the excellent compatibility of CMC with the starch surface. Noticeably, the cavitation problem is commonly present in carbohydrate matrices coated with lipidic coatings, like beeswax (Chaireh et al., 2020; Reis et al., 2018). Moreover, the total preservation of the inner structure of the starch matrix highlighted the great efficacy of the selected coating (5 wt% CMC) in preventing the entrance of water, see Fig. S5. Contrary to the porous starch-based composite coated with the aqueous solution of PVA polymer (5 wt%) reported in Zhang et al. (2022), which displayed cell collapse near the surface as a result of the gradual penetration of water.

The values of the samples' density displayed in Fig. 5 (e) revealed that the coating slightly increased this feature from $1.02 \text{ g/cm}^3 \pm 0.09 \text{ g/cm}^3$ for PS to $1.21 \text{ g/cm}^3 \pm 0.07 \text{ g/cm}^3$ for PS_CMC, and from $0.61 \text{ g/cm}^3 \pm 0.11 \text{ g/cm}^3$ for PS_CA to $0.91 \text{ g/cm}^3 \pm 0.09 \text{ g/cm}^3$ for PS_CA_CMC samples, independently of the presence of Ath. It is worth noticing that the density obtained with the starch citration was comparable with some pristine or functionalized starch foams found in the literature, such as the ones disclosed by Han et al. (2023), Pornsuk-somboon et al. (2016), Tacha et al. (2023), who reported densities that ranged from 0.2 g/cm^3 to 0.6 g/cm^3 . The density of the composites (PS_CMC and PS_CA_CMC) was acceptable when compared with analogous "bifunctional" systems with a potential application for food packaging, such as the cassava starch-poly (lactic acid) trays coated with

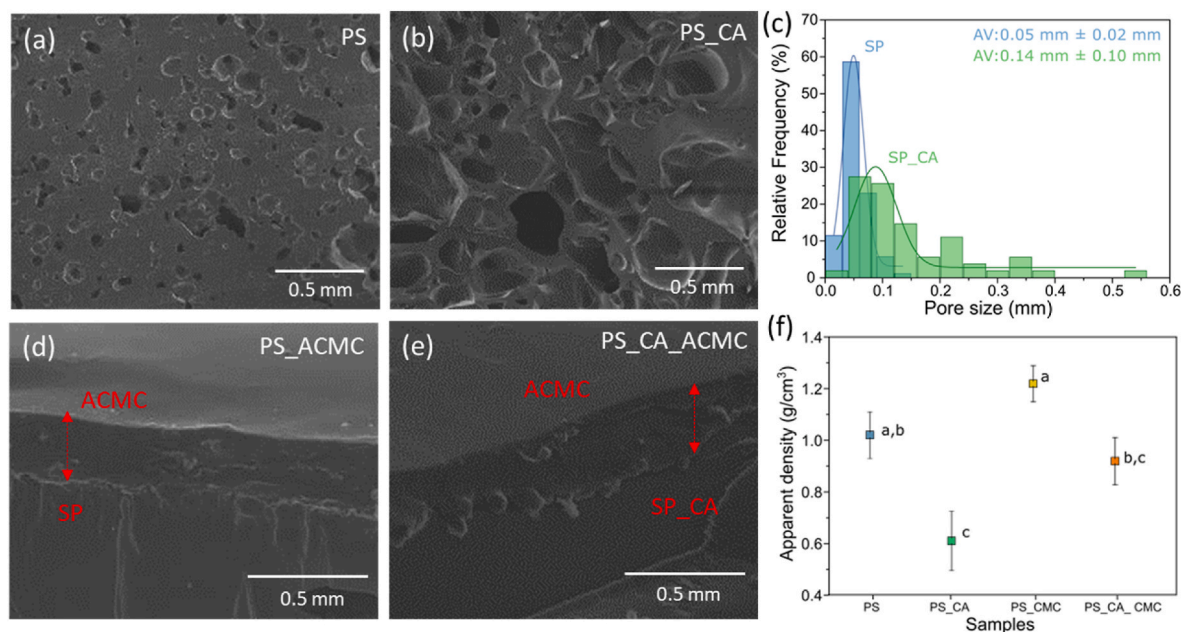


Fig. 5. The SEM cross-section images of the (a) PS, (b) PS_CA, (c) PS_ACMC, (d) PS_CA_ACMC. The coating thickness is highlighted in red. (f) The pore-size distribution diagram, and (e) the apparent density values. The same letters indicate non-significant differences among the results according to Tukey's test ($p < 0.05$).

beeswax reported by Reis et al. (2018), which displayed densities varying from 1.19 g/cm³ to 1.27 g/cm³ for uncoated and coated samples, respectively.

3.5. Thermal degradation of samples

The TGA and DTG of PS, PS_CA, PS_CMC, PS_CA_CMC and CMC are represented in Fig. S5, while all the thermal parameters obtained from these curves are registered in Table 2. In Fig. S6(a, b), the TGA and DTG curves of PS displayed the two main weight loss steps, typical of starch: the first weight loss step occurred below 200 °C and was associated with the volatilization of water molecules, while the thermal decomposition of the starch backbone was manifested in the range of 250–360 °C (Prabhakar et al., 2017).

As observed in Table 2, the thermal degradation curve of PS_CA evidenced the strong influence of the esterification on the thermal degradation properties. While the onset degradation temperature (T_{10}) was upshifted almost 100 °C with respect to PS (from 80 °C to 178 °C), the T_{max} (temperature at the maximum mass loss rate) decreased at around 20 °C (from 308 °C for PS to 284 °C for PS_CA). Such loss of thermal resistance after esterification has been already observed in other citrated-starch materials, as a result of a superior susceptibility to dehydration (Chi et al., 2024; Liu et al., 2020). This event contributed to the overall starch decomposition. The thermal resistance of PS samples was enhanced with the incorporation of the CMC coating, delaying the onset degradation temperature (T_{10}) from 80 °C to 168 °C. The T_{max} of PS was kept for PS_CMC (308 °C), while the thermal degradation properties of citrated starch were slightly weakened with the addition of the CMC coating, 284 °C for PS_CA and 270 °C for PS_CA_CMC. This last insight was justified with the formation of the minor free CA molecules during the dip-coating process, which behave as plasticizers reducing the thermal degradation temperature (Chi et al., 2024).

3.6. Mechanical properties

Fig. 6 (a) displays the results of the compression stress-strain curve of the samples. Acknowledging the remarkable plasticizing effect of moisture in such hydrophilic materials, which modifies the elasticity and stiffness of the hydrophilic biopolymers (Mali et al., 2010; Soykeabkaew et al., 2004), all samples were preconditioned in chambers for 48 h at 23 °C and 50% relative humidity following the procedure reported in our previous work (Quilez-Molina et al., 2023). The remarkable differences observed in the mechanical response of the citrated and non-citrated samples were attributed to two factors: the microstructure and the chemical bonding. The more porous PS_CA samples exhibited a typical profile of hard foams, showing a first linear elasticity region up to the elastic limit (a strain of around 20 %), followed by a slight plateau which is associated with plastic deformation (Kim et al., 2021; Miranda-Valdez et al., 2023). However, the stress-strain curve of PS, with fewer and smaller pores, was more similar to the behavior of a solid bulk, as observed in our previous work (Quilez-Molina et al., 2024). In Fig. 6 (b), the compression modulus of PS was measured at 189 kPa, which substantially decayed for PS_CA samples to 28.5 kPa. The irregular and larger pores could explain the comparatively poorer

Table 2

Thermal parameters obtained from the thermal degradation curves of S powder, PS, PS_CA, PS_CMC, PS_CA_CMC. T_{10} corresponded to the temperature at 10 % mass loss, while T_{max} to the temperature at the maximum mass loss rate.

Sample	T_{10} (°C)	T_{max} (°C)	Residual mass at 800 °C (wt.%)
PS	80	308	8.63
PS_CA	178	284	21.17
PS_CMC	163	308	12.72
PS_CA_CMC	178	270	21.77
CMC	82	251	0

mechanical properties, together with the overall reduction of the hydrogen bond interaction with the esterification (see FTIR results in Fig. 2 (b)) (Chaireh et al., 2020; Quilez-Molina et al., 2024; Tapia-Blácido et al., 2022). However, the properties found for PS_CA are comparable with the mechanical properties of expanded PS foam (EPS), widely used for packaging, which has a compression modulus of around 45 kPa (Chaireh et al., 2020; Tapia-Blácido et al., 2022). After the application of a CMC coating, a noticeable reduction in the compression modulus of PS was observed, from 189 kPa to 128 kPa.

The lack of significant chemical modifications (e.g., hydrolysis) or any damage in the cell structure of the CMC-PS sample (see the infrared, TGA or SEM analysis), may suggest that the new bonding interaction between the starch molecules and the CMC coating could have diminished the inner molecular network of the sample resulting in an overall weakening of the compressive strength (Dai et al., 2020; Poudel et al., 2023). Noticeably, the loss of mechanical strength is a general tendency observed in other bifunctional starch materials, independently of the nature of the coating, such as the hydrophilic PVA (Zhang et al., 2022) or hydrophobic beeswax (Chaireh et al., 2020). In contrast, non-significant differences were observed in the compression moduli of PS_CA and PS_CA_CMC composites.

3.7. Water resistance properties and hydrophilic characteristics

The great hydrophilic character of starch can be translated into poor water resistance which can strongly limit the applicability of this biopolymer in several fields (Karma et al., 2022; Tapia-Blácido et al., 2022). In Fig. 7 (a), the PS displays a moisture content of around 8 %, which decreased by more than 50 % after citration (PS_CA) and coating (PS_CMC), obtaining values around 3 % of moisture. This substantial reduction was attributed to the lack of available OH groups that react with water, as observed by FTIR and TGA. In the case of PS_CA, this occurred through the substitution of OH groups by the citrate group that crosslinked with a neighbouring starch chain, or through hydrogen bonds in the case of the CMC coating (Gutiérrez, 2018). The CMC coating did not significantly affect the moisture content of the PS_CA samples.

The values of water uptake (%) obtained after immersing the samples for 24 h in water are reported in Fig. 7 (b). The considerable increment of the swelling features with the esterification (PS_CA) was already observable from the 2 h after the water immersion, see Fig. S7 of Supporting information. Results collected after 24 h indicated the superior water absorption capability of PS_CA, 90 % for PS_CA against 45 % for PS. This result was associated with the higher porosity of PS_CA samples, especially with the open cells, which enhanced the water entrance and its diffusion inside the matrix (Bergel et al., 2021; Quilez-Molina et al., 2024; Zhang, Han, & Zhou, 2023). Contrary to the denser and more compact structure of PS, which impeded the water penetration and propagation. The slight increment in the water absorption of coated samples (PS_CMC and PS_CA_CMC) was considered irrelevant after the statistical study. It is worth mentioning that moderate values of water uptake are desirable for absorbing the leak of liquids released by the foodstuff during storage, which could negatively affect consumer acceptance.

The results of the solubility test represented in Fig. 7 (c) showed that PS displayed around 38%, characteristic of starch foams. Remarkably, the starch citration (PS_CA) reduced the solubility to around 23%. As explained above, the esterification involved a decrease in the free OH groups that interact with water, according to the high substitution degree (SD: 0.44 % ± 0.0 %) (Zhang, Han, & Zhou, 2023). Non-significant changes were observed in terms of solubility for PS and PS_CMC. Contrarily, the coating with CMC substantially increased the water solubility of the citrated samples (from 23 % for PS_CA to 38 % for PS_CA_CMC). The higher water solubility of PS_CA_CMC was mainly associated with the weaker interaction between the CMC and the CA-starch matrix because of the loss of OH groups in the starch after the

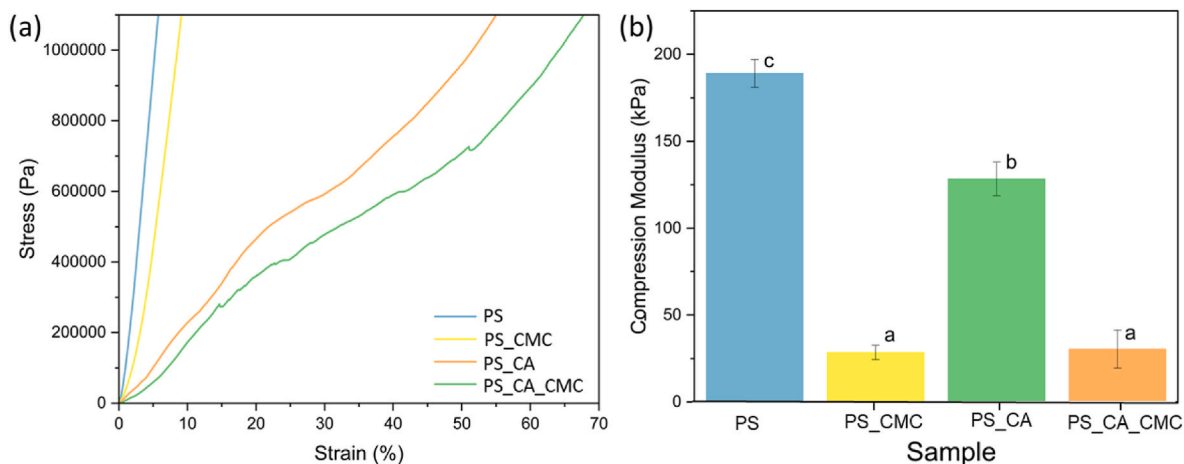


Fig. 6. Mechanical properties assayed in compression. (a) Stress (Pa) vs Strain (%) curves, (b) compression modulus (kPa) of PS, PS_CA, PS_CMC, and PS_CA_CMC. The same letters indicate non-significant differences among the results according to Tukey's test ($p < 0.05$).

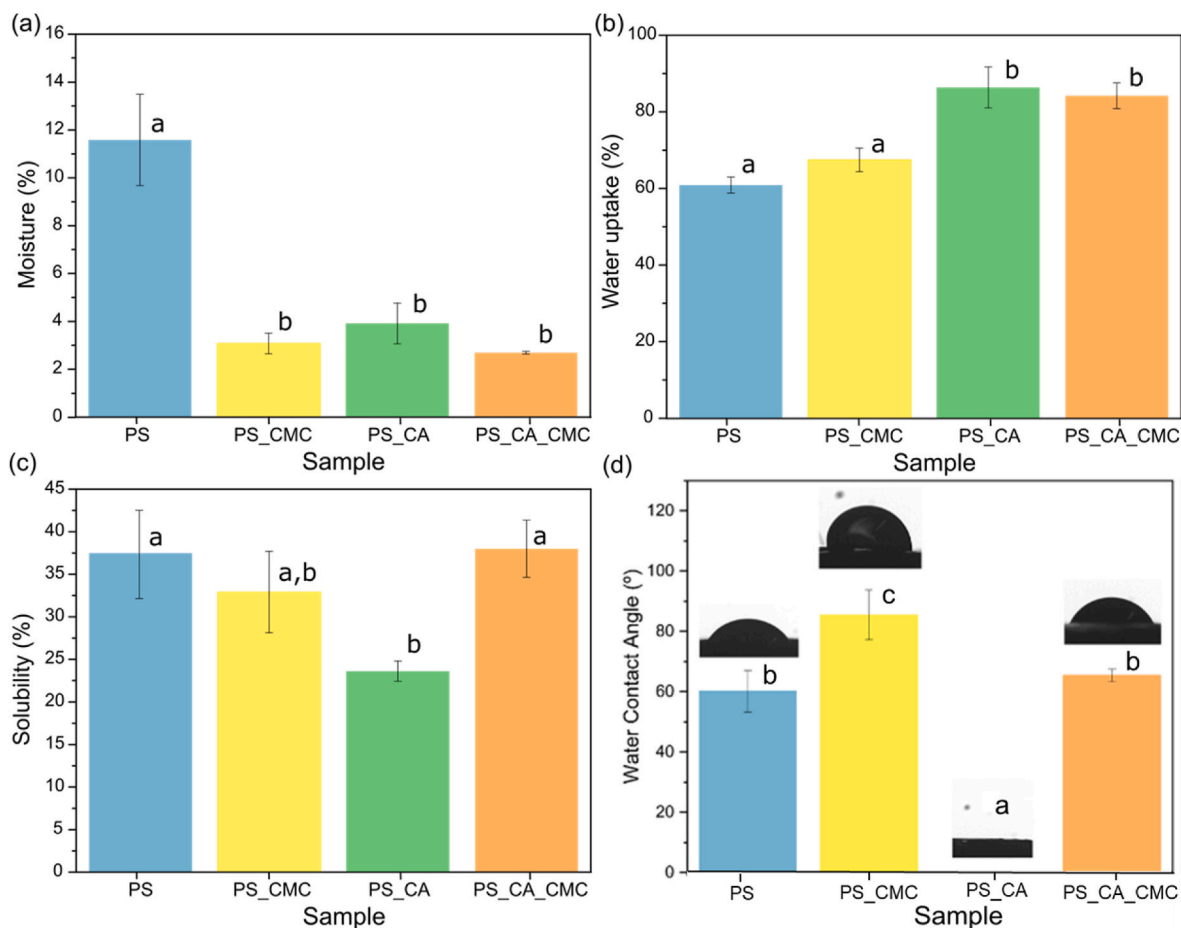


Fig. 7. Samples' interaction with water. (a) Moisture content (%), (b) water uptake (%), (c) solubility in water (%), and (d) water contact angle (°). The same letters indicate non-significant differences among the results according to Tukey's test ($p < 0.05$).

cross-linking (see the FTIR results), as well as the partial hydrolysis occurred during the dip-coating. As a result, water could interact more easily with the CMC coating causing the loss of cohesiveness. The values of solubility were comparable with sustainable polymeric trays composed of thermoplastic cassava starch and hydrophobic polylactic acid and coated with lipidic beeswax (from about 23 to 29 %) (Reis et al., 2018), and with the solubility obtained in cassava starch foam

coated with beeswax after being immersed in water for 30 min (Chaireh et al., 2020).

Fig. 7 (d) displays the values of the static water contact angle of the samples. This test gives information about the hydrophilicity nature of the sample's surface and the water wettability (Akhtar et al., 2024; Lupina et al., 2022). Results showed that PS exhibited a water contact angle of 60° showing a hydrophilic surface due to the availability of the

OH groups (Yang et al., 2020). Remarkably, after CA modification the contact angle remained undetectable probably because of the superior porosity that absorbed the drop immediately after contact. This high hydrophilicity enhanced the sample wettability, justifying the high amount of water absorbed (around 90 %) (Łupina et al., 2022). Regarding the coated samples, CMC coating prevented the water drop absorption and displayed higher contact angles of 85° for PS_CMC and 65° for PS_CA_CMC. The hydrogen bonding formed between the CMC coating and the starch reduced the availability of the free OH groups to interact with water reducing the interfacial wettability and obtaining a moderate hydrophobic behavior (Łupina et al., 2022). It is worth noting that the higher wettability (lower contact angle) in PS_CA_CMC confirmed that PS_CA displayed a weaker interaction with CMC, in agreement with the results obtained from the solubility test and FTIR.

3.8. pH-sensing properties of bifunctional materials

Anthocyanins are characterized by undergoing structural modifications depending on pH, which results in a prevailing colouration for a certain pH, usually from red/pink to yellow/green with an increase in pH value (Yong & Liu, 2020). Anthocyanins are found in equilibrium mixtures of structures that include the flavylium cation, hemiacetal, chalcone, quinoidal bases, and anionic quinoidal bases, some of them reported in Fig. 8 (a). As said above, the presence of a predominant molecule at a certain pH provides a characteristic colour, differentiable in a wide range of pH values. The pH-colour sensing response of anthocyanins has been widely used in several research activities, ranging from smart food packaging (Yong & Liu, 2020; Zhang et al., 2020) to wound healing and pharmaceutical applications (Khoo et al., 2017).

The visual colour changes in coated starch samples (PS_ACMC and PS_CA_ACMC), and the CMC film containing Ath (labelled as ACMC), used as the control, were measured after immersion in different aqueous buffer solutions with pH values ranging from 6 to 11.5. The results, represented in Fig. 8 (b), showed that ACMC films and PS_ACMC composites exhibited a rapid and stable colour change response when immersed in the buffer solutions, while PS_CA_ACMC preserved the same colouration in all experiments. The colour change was appreciable after 30 s of immersion, however, the colour change continued during

the wetting and diffusion of the aqueous buffer through the sample until it dried, when the colouration acquired kept stable. The colours obtained coincided with those reported in the literature for anthocyanins from grapes (Kan et al., 2022).

The video included in Multimedia Supporting Information visually shows the colour changes for composites after immersion in a solution pH 10.5, where the fast response can be appreciated. The lack of response in PS_CA_CMC was linked to the stronger and more stable ionic interaction with the anionic carboxylate groups shown in the scheme of Fig. 4 (c).

Fig. 8 (c) shows the total colour change (ΔE) of the samples in comparison with the dry sample and the starch composites when they were immersed in the buffer solutions. Generally, a greater ΔE^* value provides a better visual colour variation, and the naked eye does not distinguish colour changes with $\Delta E < 5$ (Quilez-Molina et al., 2021b). The PS_ACMC and ACMC exhibited significant colour changes visible to the naked eye in a wide range of pH (ACMC from pH 6 and PS_ACMC from pH 8). The more appreciable colour change in the control ACMC film was attributed to the inherent white colour of the sample, which interfered with the colour acquired by the active coating. As said before, this feature is very useful for an application as real-time freshness indicator packaging for meats and seafoods (fatty foods), as their spoilage results into the release of basic volatile molecules that gradually increase the pH, usually from 6 to 8 of pH (Merino et al., 2022; Quilez-Molina et al., 2021). Therefore, the visible colour change of PS_ACMC in this range confirmed the suitability of this material for detecting food spoilage. In addition to this, the colour acquired did not change after being for several weeks under the hood, highlighting the great colour stability and the reliable response of the material.

3.9. Migration of antioxidants in hydrophobic food simulant

The studies of migration and antioxidant properties of food packaging are critical to ensure food safety. The chemical composition of fatty foods like meat and seafood is susceptible to oxidative deterioration, which leads to off-odours, rancidity, and modification of physical characteristics of the fresh product. This set of oxidation reactions, named lipid oxidation, is the most crucial quality parameter in fatty

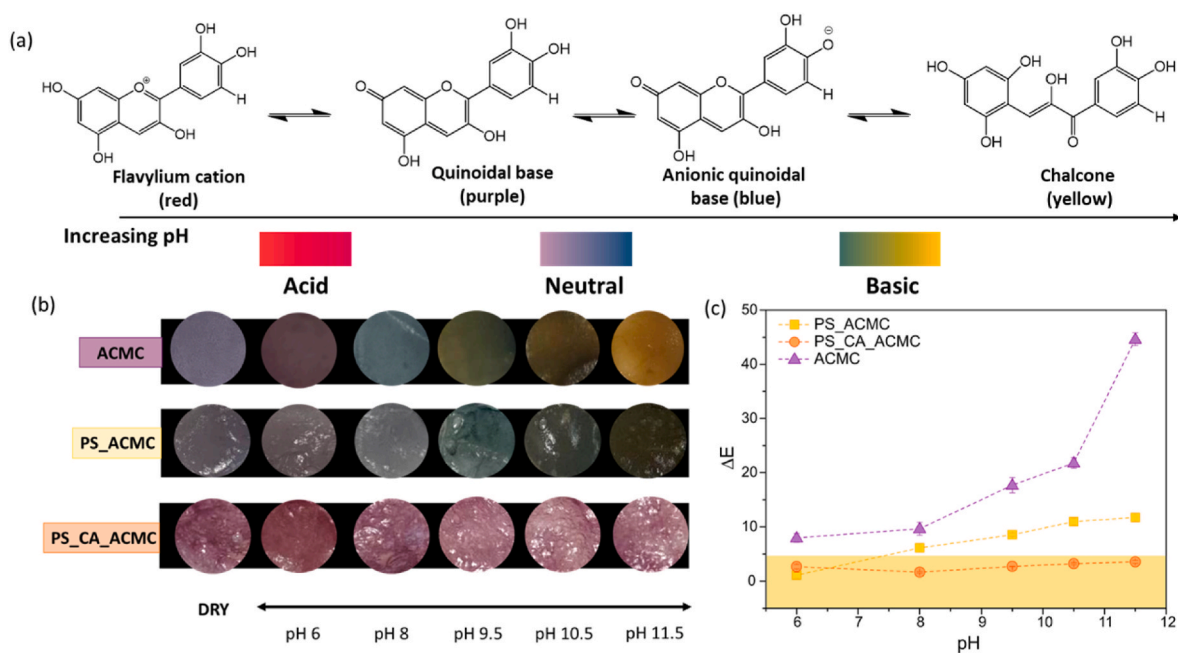


Fig. 8. pH-sensing ability of ACMC-starch composites. (a) The structure and characteristics of some of the anthocyanin's species at different pH (from 6 to 11.4 pH). (b) Photographs of the colour change as function of pH in coated samples and the control ACMC film. (c) The total colour change (ΔE) of samples with respect to the control ACMC sample as a function of pH.

foods, and it can be prevented by incorporating antioxidant molecules, such as Ath, into the packaging (Merino et al., 2022). The antioxidant properties of the PS_ACMC and PS_CA_ACMC composites and their controls, Ath, APMC, were tested in a fatty food simulant (95 % ethanol) after 24 h of immersion and represented as the radical scavenging activity (RSA) in Fig. 9 (a). Results showed that the addition of Ath improved the antioxidant response by about 60 % for PS_ACMC and 30% for PS_CA_ACMC, when compared with PS and PS_CA, respectively. Interestingly, the antioxidant response was substantially superior in PS_CA_ACMC as a consequence of the antioxidant properties of the low-quantity residual CA molecules resulting from the partial hydrolysis when the sample dipped in the aqueous solution of CMC (Zhang, Han, & Zhou, 2023). Indeed, the capability of CA to upgrade the antioxidant response in films for food packaging has been also observed in other works (Ounkaew et al., 2018). Finally, the antioxidant capability of the materials presented in this work was comparable to CMC films loaded with 10 % blueberry anthocyanin-rich extract (Sganzerla et al., 2021). Interestingly, the UV-Vis spectra of the overmentioned food simulant of Fig. 9 (b) showed minimal absorbance in the characteristic absorption peaks of the Ath at 530 and 282 nm in the spectra of the Ath, APMC, PS_ACMC and PS_CA_ACMC, indicating that the release of Ath was insignificant. Similar results have been already observed in other smart anthocyanins-CMC composite films (Liang et al., 2019; Sadi & Ferfera-Harrar, 2023), who argued that it was caused by the good anchorage of the Ath with the CMC matrix. The lack of migration indicated that the antioxidant response observed was due to the contact between the radical molecule and the surface of the sample. This result is seen as an advantage here, since the migration of colorful Ath molecules or pigments from the package to the food is undesirable, as it can modify the physical aspect of the food reducing its attractiveness for consumption (Yong & Liu, 2020).

3.10. Shrimp spoilage detection

In line with the rapid and clear colourimetric response against the pH of the PS_ACMC sample, the next study evaluates the capability of these samples in detecting shrimp spoilage. Fig. 10 (a–d) displays the photographs of the PS_ACMC trays ($8.3 \times 10 \times 3 \text{ cm}^3$) used for monitoring the shrimp freshness under room conditions (average temperature of 8°C and 55 % humidity). For this experiment, the cleaned shrimp were put on the PS_ACMC trays and covered with a plastic bag of PE.

After 24 h of experiment, the colour of the tray changed from violet to blue-greenish in the zones that were in contact with the shrimp. However, on the second day of the test, the blue was expanded to the rest of the sample, while the same zone in contact with the shrimp (marked

with a red circle) appeared slightly brownish. The total colour change (ΔE) represented in Fig. 10 (e) confirmed that the colour changes were visible to naked-eye ($\Delta E > 5$) after the first day, from violet to blue-greenish, and that it did not undergo notable variations after 24 h. These colours coincided with the colourimetric response obtained with the gradual increase in pH reported in the previous experiment, Fig. 8. Moreover, the bulky response indicated that the sample was also sensitive to the basic gases emitted by the spoiled seafood. Indeed, when the samples were uncovered, an unpleasant smell confirmed the spoilage of the shrimps. The rapid and effective response obtained is greatly significant because it evidenced that these samples were able to indicate the degree of spoilage when the food was hermetically stored (i.e., not detectable by smelling).

4. Conclusions

In this work, the fabrication of a unique fully bio-based bifunctional and sustainable material with the capability for detecting seafood spoilage has been successfully characterized and developed. Remarkably, this novel approach allowed the coexistence of the two systems, porous starch matrix (neat or functionalized) and CMC-Ath, obtaining the benefits of both components. On the one side, the porous starch matrix provided structural support and stability to the composite, providing an outstanding mechanical resistance (reaching up to 5 times more than commercial expanded polystyrene foam). Instead, CMC acted as a host complex that effectively anchored the active natural anthocyanins, conferring efficient colourimetric pH-sensing properties and ensuring a long-term response. It is worth mentioning that, contrary to other systems found in literature, these biopolymers displayed a perfect synergy with no voids or cavitation between the two phases that could weaken some functional features of the biocomposite.

Additionally, the high versatility and potential of microwave irradiation to promote chemical reactions were profited by inducing the cross-linking citration reaction on the starch matrix, in parallel with the starch expansion and foaming. This process was intended to enhance some characteristics of the starch matrix and, consequently, of the bifunctional biocomposite. As expected, this reaction involved the improvement of the starch properties by increasing water resistance and reducing the material density. However, when coated with Ath-CMC, the citration was shown to inhibit the pH-responsive properties of the Ath. A superior fixation of the Ath molecules to the CMC due to the presence of citric acid molecules justified this outcome.

Despite this variable pH-sensitive response, both composites exhibited moderate antioxidant activity when immersed in a fatty food simulant. This experiment also showed that the colorful antioxidant was

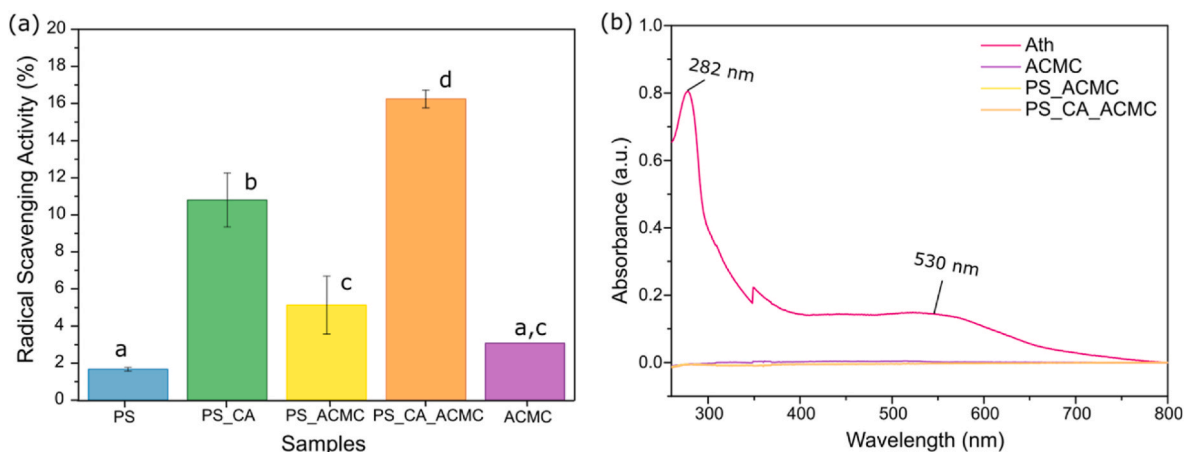


Fig. 9. Assessment of samples for active packaging. (a) The RSA (%) against DPPH radical for PS, PS_CA, PS_ACMC, PS_CA_ACMC, and APMC. (b) The UV-vis spectra of the Ath (pink) and 24 h-extract solutions (fatty food simulant) of APMC, PS_ACMC and PS_CA_ACMC samples, represented in violet, yellow and orange, respectively.

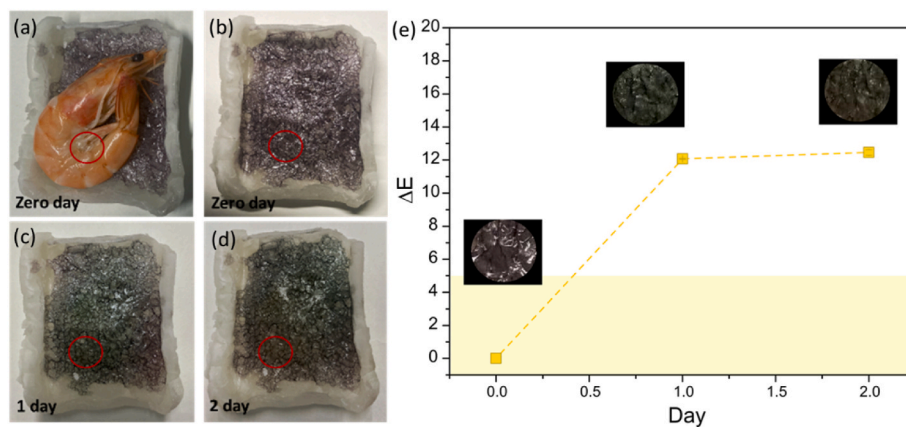


Fig. 10. (a–d) The photographs of the PS_ACMC trays at different time points of the test. The red circles indicated the zone evaluated for the colourimetric analysis. (e) The total colour change (ΔE) of the sample as a function of the day.

not released to the food simulant, which is especially important to ensure the preservation of the characteristic food appearance and long-term functional effectiveness. Finally, the freshness monitoring capability of fabricated trays of PS_ACMC samples was tested in a real-time experiment using a shrimp as a specimen. Results showed that an effective and visible to naked-eye colour change was accomplished after only 24 h, underscoring the high potential of the biocomposite to be used as a real-time colourimetric freshness indicator for seafood. Concluding, the positive and encouraging results validate the efficacy of the novel material developed on this work. While Ath was selected as the active molecule to obtain freshness-monitoring properties, the chemical structure of CMC allows the encapsulation of a diverse range of active molecules. As such, this method hold promise for sustainable and smart food packaging applications.

Funding

A. Q. would like to thank the Spanish Ministry of Universities and the Next Generation EU-Recovery for funding the post-doctoral grant “Margarita Salas”. D. M. thanks for the Emakiker grant awarded by POLYMAT and Fellows Gipuzkoa, FA/OF 156/2023, funded by the Provincial Council of Gipuzkoa.

CRedit authorship contribution statement

Ana Isabel Quilez-Molina: Writing – original draft, Visualization, Investigation, Data curation, Conceptualization. **Danila Merino:** Writing – review & editing, Validation, Data curation, Conceptualization. **Michel Dumon:** Writing – review & editing, Supervision, Project administration.

Declaration of competing interest

The authors declare that they have no known competing financial interests or personal relationships that could have appeared to influence the work reported in this paper.

Data availability

Data will be made available on request.

Acknowledgements

The authors gratefully acknowledge Jean-Marc Tallon, from Department of Science et Genie des Matériaux (IUT Bordeaux) for the technical assistance in SEM observations, as well as Cybille Rossy from the Center d’Etude Structurale et d’Analyse des Molécules Organiques

(CESAMO) for the solid ^{13}C NMR analysis.

Appendix A. Supplementary data

Supplementary data to this article can be found online at <https://doi.org/10.1016/j.foodhyd.2024.110114>.

References

- Akhtar, H. M. S., Zhao, Y., Li, L., & Shi, Q. (2024). Novel active composite films based on carboxymethyl cellulose and sodium alginate incorporated with phycocyanin: Physico-chemical, microstructural and antioxidant properties. *Food Hydrocolloids*, 147, Article 109440. <https://doi.org/10.1016/j.foodhyd.2023.109440>
- Alsahag, M., Alisaac, A., Al-Hazmi, G. A. A., Pashameah, R. A., Attar, R. M. S., Saad, F. A., & El-Metwaly, N. M. (2023). Preparation of carboxymethyl cellulose/polyvinyl alcohol wound dressing composite immobilized with anthocyanin extract for colorimetric monitoring of wound healing and prevention of wound infection. *International Journal of Biological Macromolecules*, 224, 233–242. <https://doi.org/10.1016/j.ijbiomac.2022.10.119>
- Anugrah, D. S. B., Darmalim, L. V., Sinanu, J. D., Pramitasari, R., Subali, D., Prasetyanto, E. A., & Cao, X. T. (2023). Development of alginate-based film incorporated with anthocyanins of red cabbage and zinc oxide nanoparticles as freshness indicator for prawns. *International Journal of Biological Macromolecules*, 251, Article 126203. <https://doi.org/10.1016/j.ijbiomac.2023.126203>
- Bakierska, M., Molenda, M., Majda, D., & Dziembaj, R. (2014). Functional starch based carbon aerogels for energy applications. *Procedia Engineering*, 98, 14–19. <https://doi.org/10.1016/j.proeng.2014.12.481>
- Bergel, B. F., Araujo, L. L., & Santana, R. M. C. (2021). Effects of the addition of cotton fibers and cotton microfibers on the structure and mechanical properties of starch foams made from potato starch. *Carbohydrate Polymer Technologies and Applications*, 2, Article 100167. <https://doi.org/10.1016/j.carpta.2021.100167>
- Brasoveanu, M., & Nemtanu, M. R. (2014). Behaviour of starch exposed to microwave radiation treatment. *Starch/Staerke*, 66(1–2), 3–14. <https://doi.org/10.1002/star.201200191>
- Cai, M., Zhong, H., Li, C., Aliakbarlu, J., Zhang, H., Cui, H., & Lin, L. (2022). Application of composite coating of Nostoc commune Vauch polysaccharides and sodium carboxymethyl cellulose for preservation of salmon fillets. *International Journal of Biological Macromolecules*, 210, 394–402. <https://doi.org/10.1016/j.ijbiomac.2022.05.051>
- Camani, P. H., Gonçalves, M. G. M., Barbosa, R. F. S., & Rosa, D. S. (2021). Comprehensive insight of crosslinking agent concentration influence on starch-based aerogels porous structure. *Journal of Applied Polymer Science*, 138(34), Article 50863. <https://doi.org/10.1002/app.50863>
- Camani, P. H., Midhun Dominic, C. D., Parra, D. F., Maltez, H. F., & Rosa, D. S. (2023). Divalent metal ion removal from simulated water using sustainable starch aerogels: Effect of crosslinking agent concentration and sorption conditions. *International Journal of Biological Macromolecules*, 226, 628–645. <https://doi.org/10.1016/j.ijbiomac.2022.11.308>
- Chaireh, S., Ngasatool, P., & Kaewtatip, K. (2020). Novel composite foam made from starch and water hyacinth with beeswax coating for food packaging applications. *International Journal of Biological Macromolecules*, 165, 1382–1391. <https://doi.org/10.1016/j.ijbiomac.2020.10.007>
- Chen, F., Xie, F., Liu, P., & Chen, P. (2019). Structure, thermal stability and suspension rheological properties of alcohol-alkali-treated waxy rice starch. *International Journal of Biological Macromolecules*, 134, 397–404. <https://doi.org/10.1016/j.ijbiomac.2019.05.009>
- Chi, W., Cao, L., Sun, G., Meng, F., Zhang, C., Li, J., & Wang, L. (2020). Developing a highly pH-sensitive κ -carrageenan-based intelligent film incorporating grape skin

- powder via a cleaner process. *Journal of Cleaner Production*, 244, Article 118862. <https://doi.org/10.1016/j.jclepro.2019.118862>
- Chi, Y., Maitland, E., & Pascall, M. A. (2024). The effect of citric acid concentrations on the mechanical, thermal, and structural properties of starch edible films. *International Journal of Food Science and Technology*. <https://doi.org/10.1111/ijfs.16933>
- Ciaramitaro, V., Piacenza, E., Meo, P. L., Librici, C., Calvino, M. M., Conte, P., Lazzara, G., & Chillura Martino, D. F. (2023). From micro to macro: Physical-chemical characterization of wheat starch-based films modified with PEG200, sodium citrate, or citric acid. *International Journal of Biological Macromolecules*, 253, Article 127225. <https://doi.org/10.1016/j.ijbiomac.2023.127225>
- Cuba-Chiem, L. T., Huynh, L., Ralston, J., & Beattie, D. A. (2008). In situ particle film ATR FTIR spectroscopy of carboxymethyl cellulose adsorption on talc: Binding mechanism, pH effects, and adsorption kinetics. *Langmuir*, 24(15), 8036–8044. <https://doi.org/10.1021/la800490t>
- Dai, H., Li, X., Du, J., Ma, L., Yu, Y., Zhou, H., Guo, T., & Zhang, Y. (2020). Effect of interaction between sorbitol and gelatin on gelatin properties and its mechanism under different citric acid concentrations. *Food Hydrocolloids*, 101, Article 105557. <https://doi.org/10.1016/j.foodhyd.2019.105557>
- Diop, C. I. K., Beltran, S., Sanz, M. T., Garcia-Tojal, J., & Trigo-lopez, M. (2023). Designing bilayered composite films by direct agar/chitosan and citric acid-crosslinked PVA/agar layer-by-layer casting for packaging applications. *Food Hydrocolloids*, 144, Article 108987. <https://doi.org/10.1016/j.foodhyd.2023.108987>
- Ge, J., Yue, P., Chi, J., Liang, J., & Gao, X. (2018). Formation and stability of anthocyanins-loaded nanocomplexes prepared with chitosan hydrochloride and carboxymethyl chitosan. *Food Hydrocolloids*, 74, 23–31. <https://doi.org/10.1016/j.foodhyd.2017.07.029>
- Golachowski, A., Drożdż, W., Golachowska, M., Kapelko-Zeberska, M., & Raszewski, B. (2020). Production and properties of starch citrates—current research. *Foods*, 9(9), 1311. <https://doi.org/10.3390/foods9091311>
- Gutiérrez, T. J. (2018). Active and intelligent films made from starchy sources/blackberry pulp. *Journal of Polymers and the Environment*, 26(6), 2374–2391. <https://doi.org/10.1007/s10924-017-1134-y>
- Han, J. H., Lee, J., Kim, S. K., Kang, D. H., Park, H. B., & Shim, J. K. (2023). Impact of the amylose/amylopectin ratio of starch-based foams on foaming behavior, mechanical properties, and thermal insulation performance. *ACS Sustainable Chemistry & Engineering*, 11(7), 2968–2977. <https://doi.org/10.1021/acscuschemeng.2c06505>
- Hassan, M. M., Tucker, N., & Le Guen, M. J. (2020). Thermal, mechanical and viscoelastic properties of citric acid-crosslinked starch/cellulose composite foams. *Carbohydrate Polymers*, 230, Article 115675. <https://doi.org/10.1016/j.carbpol.2019.115675>
- Hong, J. S., Chung, H. J., Lee, B. H., & Kim, H. S. (2020). Impact of static and dynamic models of semi-dry heat reaction on the characteristics of starch citrates. *Carbohydrate Polymers*, 233, Article 115853. <https://doi.org/10.1016/j.carbpol.2020.115853>
- Hu, A., Chen, X., Wang, J., Wang, X., Zheng, J., & Wang, L. (2021). Effects on the structure and properties of native corn starch modified by enzymatic debranching (ED), microwave assisted esterification with citric acid (MCAE) and by the dual ED/MCAE treatment. *International Journal of Biological Macromolecules*, 171, 123–129. <https://doi.org/10.1016/j.ijbiomac.2021.01.012>
- Jyothi, A. N., Moorthy, S. N., Sreekumar, J. N., & Rajasekharan, K. N. (2007). Studies on the properties of citrate derivatives of cassava (*Manihot esculenta* Crantz) starch synthesized by microwave technique. *Journal of the Science of Food and Agriculture*, 87(5), 871–879. <https://doi.org/10.1002/jpsa.2800>
- Kan, J., Liu, J., Xu, F., Yun, D., Yong, H., & Liu, J. (2022). Development of pork and shrimp freshness monitoring labels based on starch/polyvinyl alcohol matrices and anthocyanins from 14 plants: A comparative study. *Food Hydrocolloids*, 124, Article 107293. <https://doi.org/10.1016/j.foodhyd.2021.107293>
- Karma, V., Gupta, A. D., Yadav, D. K., Singh, A. A., Verma, M., & Singh, H. (2022). Recent developments in starch modification by organic acids: A review. *Starch/Stärke*, 74(9–10), Article 2200025. <https://doi.org/10.1002/star.202200025>
- Katoh, E., Murata, K., & Fujita, N. (2020). ¹³C CP/MAS NMR can discriminate genetic backgrounds of rice starch. *ACS Omega*, 5(38), 24592–24600. <https://doi.org/10.1021/acsomega.0c03113>
- Kho, H. E., Azlan, A., Tang, S. T., & Lim, S. M. (2017). Anthocyanidins and anthocyanins: Colored pigments as food, pharmaceutical ingredients, and the potential health benefits. *Food & Nutrition Research*, 61(1), Article 1361779. <https://doi.org/10.1080/16546628.2017.1361779>
- Kim, J. D., Kim, J. H., Lee, D. H., Yeom, D. J., & Lee, J. M. (2021). Synthesis and investigation of cryogenic mechanical properties of chopped-glass-fiber-reinforced polyisocyanurate foam. *Materials*, 14(2), 1–18. <https://doi.org/10.3390/ma14020446>
- Kim, J. Y., Lee, Y. K., & Chang, Y. H. (2017). Structure and digestibility properties of resistant rice starch cross-linked with citric acid. *International Journal of Food Properties*, 20, 2166–2177. <https://doi.org/10.1080/10942912.2017.1368551>
- Liang, T., Sun, G., Cao, L., Li, J., & Wang, L. (2019). A pH and NH₃ sensing intelligent film based on Artemisia sphaerocephala Krasch. gum and red cabbage anthocyanins anchored by carboxymethyl cellulose sodium added as a host complex. *Food Hydrocolloids*, 87, 858–868. <https://doi.org/10.1016/j.foodhyd.2018.08.028>
- Liu, Y., Liu, J., Kong, J., Wang, R., Liu, M., Strappe, P., Blanchard, C., & Zhou, Z. (2020b). Citrate esterification of debranched waxy maize starch: Structural, physicochemical and amylolysis properties. *Food Hydrocolloids*, 104, Article 105704. <https://doi.org/10.1016/j.foodhyd.2020.105704>
- Liu, B., Zhuang, J., & Wei, G. (2020a). Recent advances in the design of colorimetric sensors for environmental monitoring. *Environmental Science: Nano*, 7(8), 2195–2213. <https://doi.org/10.1039/d0en00449a>
- Lopez-Gil, A., Silva-Bellucci, F., Velasco, D., Ardantuy, M., & Rodriguez-Perez, M. A. (2015). Cellular structure and mechanical properties of starch-based foamed blocks reinforced with natural fibers and produced by microwave heating. *Industrial Crops and Products*, 66, 194–205. <https://doi.org/10.1016/j.indcrop.2014.12.025>
- Lupina, K., Kowalczyk, D., Lis, M., Raszewska-Kaczor, A., & Drozłowska, E. (2022). Controlled release of water-soluble astaxanthin from carboxymethyl cellulose/gelatin and octenyl succinic anhydride starch/gelatin blend films. *Food Hydrocolloids*, 123, Article 107179. <https://doi.org/10.1016/j.foodhyd.2021.107179>
- Ma, X., Chang, P. R., Yu, J., & Stumborg, M. (2009). Properties of biodegradable citric acid-modified granular starch/thermoplastic pea starch composites. *Carbohydrate Polymers*, 75(1), 1–8. <https://doi.org/10.1016/j.carbpol.2008.05.020>
- Ma, Q., & Wang, L. (2016). Preparation of a visual pH-sensing film based on tara gum incorporating cellulose and extracts from grape skins. *Sensors and Actuators, B: Chemical*, 235, 401–407. <https://doi.org/10.1016/j.snb.2016.05.107>
- Mali, S., Debiagi, F., Grossmann, M. V. E., & Yamashita, F. (2010). Starch, sugarcane bagasse fibre, and polyvinyl alcohol effects on extruded foam properties: A mixture design approach. *Industrial Crops and Products*, 32(3), 353–359. <https://doi.org/10.1016/j.indcrop.2010.05.014>
- Merino, D., Bellasi, P., Paul, U. C., Morelli, L., & Athanassiou, A. (2023). Assessment of chitosan/pectin-rich vegetable waste composites for the active packaging of dry foods. *Food Hydrocolloids*, 139, Article 108580. <https://doi.org/10.1016/j.foodhyd.2023.108580>
- Merino, D., Mansilla, A. Y., Gutiérrez, T. J., Casalougué, C. A., & Alvarez, V. A. (2018). Chitosan coated-phosphorylated starch films: Water interaction, transparency and antibacterial properties. *Reactive and Functional Polymers*, 131, 445–453. <https://doi.org/10.1016/j.reactfunctpolym.2018.08.012>
- Merino, D., Mansilla, A. Y., Salcedo, M. F., & Athanassiou, A. (2023). Upcycling orange peel agricultural waste for the preparation of green hydrogels as active soil conditioners. *ACS Sustainable Chemistry & Engineering*, 11(29), 10917–10928. <https://doi.org/10.1021/acscuschemeng.3c02992>
- Merino, D., Quilez-Molina, A. I., Perotto, G., Bassani, A., Spigno, G., & Athanassiou, A. (2022). A second life for fruit and vegetable waste: A review on bioplastic films and coatings for potential food protection applications. *Green Chemistry*, 24(12), 4703–4727. <https://doi.org/10.1039/d1gc03904k>
- Miranda-Valdez, I. Y., Coffeng, S., Zhou, Y., Viitanen, L., Hu, X., Jannuzzi, L., Puisto, A., Kostianen, M. A., Mäkinen, T., Koivisto, J., & Alava, M. J. (2023). Foam-formed biocomposites based on cellulose products and lignin. *Cellulose*, 30(4), 2253–2266. <https://doi.org/10.1007/s10570-022-05041-3>
- Nechita, P., & Năstac, S. M. (2022). Overview on foam forming cellulose materials for cushioning packaging applications. *Polymers*, 14(10), 1963. <https://doi.org/10.3390/polym14101963>
- Ounkaew, A., Kasemsiri, P., Kamwilaisak, K., Saengprachatanarug, K., Mongkolthanaruk, W., Souvanh, M., Pongsa, U., & Chindaprasit, P. (2018). Polyvinyl alcohol (PVA)/Starch bioactive packaging film enriched with antioxidants from spent coffee ground and citric acid. *Journal of Polymers and the Environment*, 26(9), 3762–3772. <https://doi.org/10.1007/s10924-018-1254-z>
- Panahirad, S., Daddour, M., Peighambari, S. H., Soltanzadeh, M., Gullón, B., Alirezalu, K., & Lorenzo, J. M. (2021). Applications of carboxymethyl cellulose- and pectin-based active edible coatings in preservation of fruits and vegetables: A review. *Trends in Food Science and Technology*, 110, 663–673. <https://doi.org/10.1016/j.tifs.2021.02.025>
- Peng, S., Li, F., Man, J., Li, J., Zhang, C., Ji, M., Li, J., & Wang, S. (2022). Enhancing the properties of starch-fiber foaming material by adjusting fiber length: The synergistic effect of macro-micro stress conduction. *Materials Today Communications*, 33, Article 104408. <https://doi.org/10.1016/j.mtcomm.2022.104408>
- Pornsuksomboon, K., Holló, B. B., Szécsényi, K. M., & Kaewtatip, K. (2016). Properties of baked foams from citric acid modified cassava starch and native cassava starch blends. *Carbohydrate Polymers*, 136, 107–112. <https://doi.org/10.1016/j.carbpol.2015.09.019>
- Poudel, R., Dutta, N., & Karak, N. (2023). A mechanically robust biodegradable bioplastic of citric acid modified plasticized yam starch with anthocyanin as a fish spoilage auto-detecting smart film. *International Journal of Biological Macromolecules*, 242, Article 125020. <https://doi.org/10.1016/j.ijbiomac.2023.125020>
- Prabhakar, Rehman Shah, M. N., ur, A., & Song, J. I. (2017). Improved flame-retardant and tensile properties of thermoplastic starch/flax fabric green composites. *Carbohydrate Polymers*, 168, 201–211. <https://doi.org/10.1016/j.carbpol.2017.03.036>
- Quilez-Molina, A. I., Heredia-Guerrero, J. A., Armirotti, A., Paul, U. C., Athanassiou, A., & Bayer, I. S. (2020). Comparison of physicochemical, mechanical and antioxidant properties of polyvinyl alcohol films containing green tea leaves waste extracts and discarded balsamic vinegar. *Food Packaging and Shelf Life*, 23, Article 100445. <https://doi.org/10.1016/j.foodps.2019.100445>
- Quilez-Molina, A. I., Le Meins, J. F., Charrier, B., & Dumon, M. (2024). Starch-fibers composites, a study of all-polysaccharide foams from microwave foaming to biodegradation. *Carbohydrate Polymers*, 328, Article 121743. <https://doi.org/10.1016/j.carbpol.2023.121743>
- Quilez-Molina, A. I., & Merino, D. (2023). From waste to resource: Methods for vegetable waste tranPSormation into sustainable plant-based bioplastics. In *Advanced applications of biobased materials* (pp. 61–110). Elsevier. <https://doi.org/10.1016/B978-0-323-91677-6.00023-4>
- Quilez-Molina, A. I., Oliveira-Salmazo, L., Amezcua-Arranz, C., López-Gil, A., & Rodríguez-Pérez, M. A. (2023). Evaluation of the acid hydrolysis as pre-treatment to

- enhance the integration and functionality of starch composites filled with rich-in-pectin agri-food waste orange peel. *Industrial Crops and Products*, 205, Article 117407. <https://doi.org/10.1016/j.indcrop.2023.117407>
- Quilez-Molina, A. I., Pasquale, L., Debellis, D., Tedeschi, G., Athanassiou, A., & Bayer, I. S. (2021). Responsive bio-composites from magnesium carbonate filled polycaprolactone and curcumin-functionalized cellulose fibers. *Advanced Sustainable Systems*, 5(10), Article 2100128. <https://doi.org/10.1002/adsu.202100128>
- Ramirez, D. O. S., Carletto, R. A., Tonetti, C., Giachet, F. T., Varesano, A., & Vineis, C. (2017). Wool keratin film plasticized by citric acid for food packaging. *Food Packaging and Shelf Life*, 12, 100–106. <https://doi.org/10.1016/j.fpsl.2017.04.004>
- Reddy, N., & Yang, Y. (2010). Citric acid cross-linking of starch films. *Food Chemistry*, 118(3), 702–711. <https://doi.org/10.1016/j.foodchem.2009.05.050>
- Reis, M. O., Olivato, J. B., Bilck, A. P., Zanela, J., Grossmann, M. V. E., & Yamashita, F. (2018). Biodegradable trays of thermoplastic starch/poly (lactic acid) coated with beeswax. *Industrial Crops and Products*, 112, 481–487. <https://doi.org/10.1016/j.indcrop.2017.12.045>
- Sadi, A., & Ferfera-Harrar, H. (2023). Cross-linked CMC/gelatin bio-nanocomposite films with organoclay, red cabbage anthocyanins and pistacia leaves extract as active intelligent food packaging: Colorimetric pH indication, antimicrobial/antioxidant properties, and shrimp spoilage tests. *International Journal of Biological Macromolecules*, 242, Article 124964. <https://doi.org/10.1016/j.ijbiomac.2023.124964>
- Sadik, T., Pillon, C., Carrot, C., & Reglero Ruiz, J. A. (2018). Dsc studies on the decomposition of chemical blowing agents based on citric acid and sodium bicarbonate. *Thermochimica Acta*, 659, 74–81. <https://doi.org/10.1016/j.tca.2017.11.007>
- Sánchez-Rivera, M. M., Núñez-Santiago, M. del C., Bello-Pérez, L. A., Agama-Acevedo, E., & Alvarez-Ramirez, J. (2017). Citric acid esterification of unripe plantain flour: Physicochemical properties and starch digestibility. *Starch/Staerke*, 69(9–10), Article 1700019. <https://doi.org/10.1002/star.201700019>
- Sganzerla, W. G., Pereira Ribeiro, C. P., Uliana, N. R., Cassetari Rodrigues, M. B., da Rosa, C. G., Ferrareze, J. P., Veeck, A. P. de L., & Nunes, M. R. (2021). Bioactive and pH-sensitive films based on carboxymethyl cellulose and blackberry (*Morus nigra* L.) anthocyanin-rich extract: A perspective coating material to improve the shelf life of cherry tomato (*Solanum lycopersicum* L. var. cerasiforme). *Biocatalysis and Agricultural Biotechnology*, 33, Article 101989. <https://doi.org/10.1016/j.bcab.2021.101989>
- Shi, R., Zhang, Z., Liu, Q., Han, Y., Zhang, L., Chen, D., & Tian, W. (2007). Characterization of citric acid/glycerol co-plasticized thermoplastic starch prepared by melt blending. *Carbohydrate Polymers*, 69(4), 748–755. <https://doi.org/10.1016/j.carbpol.2007.02.010>
- Soykeabkaew, N., Thanomsilp, C., & Suwanton, O. (2015). A review: Starch-based composite foams. *Composites Part A: Applied Science and Manufacturing*, 78, 246–263. <https://doi.org/10.1016/j.compositesa.2015.08.014>
- Tacha, S., Somord, K., Rattanawongkun, P., Intatha, U., Tawichai, N., & Soykeabkaew, N. (2023). Bio-nanocomposite foams of starch reinforced with bacterial nanocellulose fibers. *Materials Today: Proceedings*, 75, 119–123. <https://doi.org/10.1016/j.matpr.2022.12.049>
- Tapia-Blácido, D. R., Aguilar, G. J., de Andrade, M. T., Rodrigues-Júnior, M. F., & Guareschi-Martins, F. C. (2022). Trends and challenges of starch-based foams for use as food packaging and food container. *Trends in Food Science and Technology*, 199, 257–271. <https://doi.org/10.1016/j.tifs.2021.12.005>
- Tavares, K. M., de Campos, A., Mitsuyuki, M. C., Luchesi, B. R., & Marconcini, J. M. (2019). Corn and cassava starch with carboxymethyl cellulose films and its mechanical and hydrophobic properties. *Carbohydrate Polymers*, 223, Article 115055. <https://doi.org/10.1016/j.carbpol.2019.115055>
- Uttaravalli, A. N., Dinda, S., & Gidla, B. R. (2020). Scientific and engineering aspects of potential applications of post-consumer (waste) expanded polystyrene: A review. *Process Safety and Environmental Protection*, 137, 140–148. <https://doi.org/10.1016/j.psep.2020.02.023>
- Wu, C., Sun, R., Zhang, Q., & Zhong, G. (2020). Synthesis and characterization of citric acid esterified canna starch (RS4) by semi-dry method using vacuum-microwave-infrared assistance. *Carbohydrate Polymers*, 250, Article 116985. <https://doi.org/10.1016/j.carbpol.2020.116985>
- Xia, L., Wenyuan, G., Qianqian, J., Luqi, H., & Changxiao, L. (2011). Study on the morphology, crystalline structure, and thermal properties of *Fritillaria ussuriensis* Maxim. starch acetates with different degrees of substitution. *Starch/Staerke*, 63(1), 24–31. <https://doi.org/10.1002/star.201000055>
- Yang, W., He, X., Luzzi, F., Dong, W., Zheng, T., Kenny, J. M., Puglia, D., & Ma, P. (2020). Thermomechanical, antioxidant and moisture behaviour of PVA films in presence of citric acid esterified cellulose nanocrystals. *International Journal of Biological Macromolecules*, 161, 617–626. <https://doi.org/10.1016/j.ijbiomac.2020.06.082>
- Yong, H., & Liu, J. (2020). Recent advances in the preparation, physical and functional properties, and applications of anthocyanins-based active and intelligent packaging films. *Food Packaging and Shelf Life*, 26, Article 100550. <https://doi.org/10.1016/j.fpsl.2020.100550>
- Zhang, A., Han, Y., & Zhou, Z. (2023). Characterization of citric acid crosslinked chitosan/gelatin composite film with enterocin CHQS and red cabbage pigment. *Food Hydrocolloids*, 135, Article 108144. <https://doi.org/10.1016/j.foodhyd.2022.108144>
- Zhang, Y., Li, C., Fu, X., Ma, N., Bao, X., & Liu, H. (2022). Characterization of a novel starch-based foam with a tunable release of oxygen. *Food Chemistry*, 389, Article 133062. <https://doi.org/10.1016/j.foodchem.2022.133062>
- Zhang, W., Qi, X., Zhao, Y., Liu, Y., Xu, L., Song, X., Xiao, C., Yuan, X., Zhang, J., & Hou, M. (2020). Study of injectable Blueberry anthocyanins-loaded hydrogel for promoting full-thickness wound healing. *International Journal of Pharmaceutics*, 586, Article 119543. <https://doi.org/10.1016/j.ijpharm.2020.119543>
- Zhang, W., Roy, S., Assadpour, E., Cong, X., & Jafari, S. M. (2023). Cross-linked biopolymeric films by citric acid for food packaging and preservation. *Advances in Colloid and Interface Science*, 102886. <https://doi.org/10.1016/j.cis.2023.102886>
- Zhang, L., Zhang, M., Adhikari, B., & Zhang, L. (2023). Preparation and properties of citric acid-crosslinked chitosan salt microspheres through radio frequency assisted method. *Food Hydrocolloids*, 139, Article 108538. <https://doi.org/10.1016/j.foodhyd.2023.108538>
- Zhao, S., Jia, R., Yang, J., Dai, L., Ji, N., Xiong, L., & Sun, Q. (2022). Development of chitosan/tannic acid/corn starch multifunctional bilayer smart films as pH-responsive actuators and for fruit preservation. *International Journal of Biological Macromolecules*, 205, 419–429. <https://doi.org/10.1016/j.ijbiomac.2022.02.101>
- Zhong, C., Xiong, Y., Lu, H., Luo, S., Wu, J., Ye, J., & Liu, C. (2022). Preparation and characterization of rice starch citrates by superheated steam: A new strategy of producing resistant starch. *Lebensmittel-Wissenschaft & Technologie*, 154, Article 112890. <https://doi.org/10.1016/j.lwt.2021.112890>